




Amplification of turbulence through multiple planar shocks

Michael F. Zhang ^{1,2,*}, Seth Davidovits ³ and Nathaniel J. Fisch ^{1,2}

¹*Department of Astrophysical Sciences, Princeton University, Peyton Hall, Princeton, New Jersey 08544, USA*

²*Princeton Plasma Physics Laboratory, P.O. Box 451, Princeton, New Jersey 08543, USA*

³*Lawrence Livermore National Laboratory, Livermore, California 94550, USA*



(Received 28 February 2025; accepted 2 July 2025; published 14 August 2025)

We study the amplification of isotropic, incompressible turbulence through multiple planar, collisional shocks, using analytical linear theory. There are two limiting cases we explore. The first assumes shocks occur rapidly in time such that the turbulence does not evolve between shocks. Whereas the second case allows enough time for turbulence to isotropize between each shock. For the latter case, through a quasi-equation-of-state, we show that the weak multishock limit is agnostic to the distinction between thermal and vortical turbulent pressures, like an isotropic volumetric compression. When turbulence does not return to isotropy between shocks, the generated anisotropy—itsself a function of shock strength—can feedback on amplification by further shocks, altering choices for maximal or minimal amplification. In addition for this case, we find that amplification is sensitive to the shock ordering. We map how choices of shock strength can impact these amplification differences due to ordering, finding, for example, shock pairs which lead to identical mean postshock fields (density, temperature, pressure) but maximally distinct turbulent amplification.

DOI: [10.1103/dz6k-rmdx](https://doi.org/10.1103/dz6k-rmdx)

I. INTRODUCTION

The interaction of turbulence with shocks is a fundamental fluid phenomenon that is ubiquitous across a variety of fields. For example, turbulence seeded by asymmetry or Rayleigh-Taylor and Richtmyer-Meshkov instabilities in inertial confinement fusion (ICF) implosions [1–6] where shocks are used in compression and are present during stagnation [7]; accretion shocks, e.g., supernovae explosions [8–10] and star formation [11]; supersonic flight and propulsion [12].

Often, there may be multiple shocks in physical situations of interest where the interaction with turbulence or fluctuations can be important. A necessary condition for ICF is the attainment of a high areal or column density (ρR , with ρ the density and R the radius) for the fuel layer to confine the burning fuel for a sufficient time to fuse an appreciable fraction [7]. To permit the attainment of high areal density, for laser driven ICF, a sequence of shocks (e.g., 3 [13] or 4 [14]) is carefully tailored to implode the fuel while controlling the fuel heating such that it remains cold and highly compressible. These shocks can be chosen and implemented by combining modeling with dedicated experiments (e.g., Ref. [15]) to confirm the shock sequence. When, as is typically the case, the fuel is surrounded by a shell of ablator material (e.g., plastic, beryllium, or multicrystalline diamond), the ablator will also experience this rapid sequence of shocks.

If there is density nonuniformity in the target, such as grains [16–18] or in hydrocarbon foams filled with deuterium-tritium [19–22], interaction with the first shock can generate a turbulent flow field that interacts with subsequent shocks [23]. In addition, some experiments at the National Ignition Facility

(NIF) are investigating the Richtmyer-Meshkov instability (RMI) and can feature multiple planar shocks [24,25]. Related to this, there have been computational studies to understand how RMI behaves under the action of multiple shocks [26,27]. Within astrophysics, turbulence is important in understanding the structure of interstellar gas and molecular clouds, where multiple shocks may be present [28,29]. In supersonic propulsion, trains of shocks manifest within nozzles, and can interact with turbulent boundary layers [30]. In many of these cases, the conditions under which turbulence would be maximally or minimally enhanced by a sequence of multiple (or many) shocks is important to the dynamics. Here we will use a theory for shock-turbulence interaction to study this and other dynamics for multiple planar shocks.

Many works thus far have been focused on the canonical interaction of a single planar shock with isotropic turbulence [31–33]. Fundamental theoretical studies were initiated by Ribner’s linear interaction analysis (LIA) [34,35], which took a Kovasnay decomposition [36] of the turbulence into a superposition of nonpropagating vorticity modes. Through linearizing the fluid equations and Rankine-Hugoniot jump relations under the assumption of weak turbulence relative to the shock, how each mode changes across the shock can be determined. The effects can then be summed to infer properties of the downstream turbulence, including the amplification of turbulent kinetic energy.

Later works have revisited LIA and developed analytical expressions for amplification of turbulent kinetic energy in general and in certain asymptotic limits [37]. Others have made use of Moore’s results on the linear interaction of an acoustic wave with a shock [38] to adapt the analysis for upstream acoustic and entropy modes [39,40].

In this paper, we adapt Ribner’s single-shock LIA to develop an initial theory for the multishock amplifica-

*Contact author: mfzhang@princeton.edu

tion of initially isotropic (or axisymmetric), incompressible, vortical, weak turbulence. For such turbulence, good agreement on turbulent kinetic energy (TKE) amplification has been found between Ribner's single-shock LIA with direct numerical simulation (DNS) [41–43] and a wind tunnel experiment [33,44]. Whilst there have been discrepancies on the downstream anisotropy [45] and when departing from the assumptions of LIA [46–50], the otherwise good agreement motivates the use of LIA as a building block for a theory of multishock interaction with turbulence. We do this for two opposite limits where either the turbulence is allowed to isotropize between shocks, or it remains anisotropic. Taking such limits allows for the use of inviscid LIA to compute turbulent vortical spectra without concern for the details of the nonlinear, viscous evolution between each shock. The isotropy, or not, of turbulence under compression has been shown to be important for its growth in the case of uniform (metric) compression [51], and so we examine both limits here.

Our model is described further in Sec. II. We give formulas that prescribe the TKE amplification in each limit. In particular, amplifications of longitudinal (parallel to shock propagation) and lateral (perpendicular to shock propagation, parallel to shock front) components of vortical turbulence are given in the nonisotropized limit.

We compute these as functions of shock strength for various multishock compression scenarios of interest in Sec. III. General trends with shock strength are shown in each limit for a series of identical shocks, in Sec. III A. We show that weaker shocks are more efficient at amplifying turbulence for a fixed final density state. In particular, for the isotropized limit, there exists an optimal shock strength that depends only on the thermal polytropic index. In the nonisotropized limit, we will show that the preferential longitudinal enhancement of turbulence by weaker shocks sustains the continued amplification by subsequent shocks. However, a series of stronger shocks preferentially amplifies the lateral component through a refractive effect and can simultaneously suppress the longitudinal component, limiting further amplification.

We use these calculations, in Sec. III B, to inform compression energetics by acquiring polytropic indices via a turbulent quasi-equation-of-state. These indices show that the turbulent pressure in the weak-shock, isotropized limit exhibits the same adiabatic behavior as the thermal pressure for an isotropic, metric compression. In contrast, the nonisotropized case is superadiabatic in the weak shock limit. Departing from the weak shock limit reduces the polytropic indices associated with turbulent pressure in both limits, leading to subadiabatic behavior under shock compression.

One significant departure between the two limits is discovered for a series of nonidentical shocks of variable strength, in Sec. III C. We show such a scenario is noncommutative for the nonisotropized limit, whereby the amplification of TKE is sensitive to the order of the shocks. In Sec. IV, we discuss the implications of these results for experimental shock-compression scenarios, and the caveats to the assumptions made in the model.

II. MODEL

We now discuss our model for the multishock amplification of turbulence, and the simplifying assumptions used. Consider low-Mach, isotropic, homogeneous, incompressible turbulence in a compressible flow. Assuming there are no large macroscopic gradients, the dynamics are well described by the compressible Navier-Stokes equations, and one could assume an ideal gas equation of state.

The parameters that describe the flow are: density ρ , flow velocity \mathbf{v} , and thermal pressure p , which relates to the total energy, E_{total} , via the equation of state. We assume $\gamma = 5/3$ for the thermal polytropic index. The three spatial dimensions are x , y , and z , with the shock normal aligned to x . $\mathbf{v} = \bar{\mathbf{v}} + \tilde{\mathbf{v}}$ includes the background flow, $\bar{\mathbf{v}}$, and the turbulent flow, $\tilde{\mathbf{v}}$. For brevity, we will denote the turbulent kinetic portion of the energy as

$$E \doteq E_{\text{TKE}} \doteq \int d^3\mathbf{r} \frac{1}{2} \rho \tilde{\mathbf{v}}^2 = \frac{1}{2} \rho V \overline{\tilde{\mathbf{v}}^2}, \quad (1)$$

where we have used the incompressibility and homogeneity of the turbulence, assuming acoustic modes are negligible, and the bar denotes a volume average. The distinction between total turbulent kinetic energy and energy density does not matter for scenarios where the final density is fixed. However, for cases where the final density is not fixed, considering the volume averaged energy allows us to consider the shock-induced vorticity amplification separately from the compression ratio.

With appropriate initial and boundary conditions, a shock can propagate past the turbulence. Both the mean properties of the flow and the root mean square amplitude of the turbulent fluctuations will change across the shock. The strength of the shock measures how large the jumps in fluid quantities are. It can be described either by the Mach speed of the shock relative to the background flow, or any of the jumps in mean fluid properties such as the density, $m = \rho_1/\rho_0$, where the subscript refers to the background quantity after that number of shocks.

A simple setup for investigating the amplification of isotropic, incompressible turbulence after multiple planar shocks is shown in Fig. 1. We imagine choosing N shocks of given strengths, defined by their density jumps,

$$m_i \doteq \frac{\rho_i}{\rho_{i-1}}, \quad (2)$$

for shock i . The shocks are spaced such that the following shocks do not overtake the preceding shocks before propagating past the turbulent region. These density jumps, m_i , give a frame-independent measure of shock strength, whereas the Mach speeds in the laboratory frame, M'_i , to achieve a given m_i generally depend on the background flow speed immediately ahead of a shock.

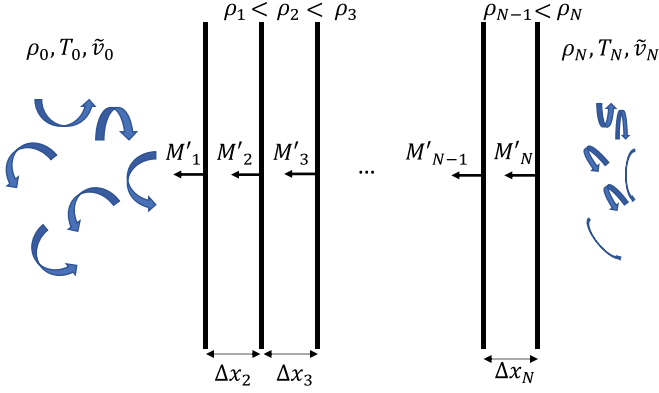


FIG. 1. Setup of problem for interaction of an initial isotropic distribution of incompressible turbulence on the left with N leftward propagating shocks. The Mach speeds of each shock in the laboratory frame, denoted by a prime, M'_i , are not the same as those used in calculating shock-jump relations, M_i , where the background flow ahead of a shock is taken to be stationary. Fluid quantities downstream of each shock are denoted by the number of the shock, with 0 denoting the initial upstream conditions. The spacing between shocks, Δx_i , can be arbitrarily adjusted such that they do not overtake each other before propagating through the turbulence.

Two cases can then be examined in this problem: (a) Spacing between shocks is short, such that the turbulence does not have sufficient time to evolve between shocks. For a turbulent turnover time, $\tau_\epsilon \sim E/(dE/dt)$ [52], this condition can be expressed as $(\Delta t_i = \Delta x_i/M'_i \ll \tau_\epsilon)$. We will refer to this as the nonisotropization case (NIC). (b) The second shock follows a sufficient distance behind the first shock such that the anisotropic, shocked turbulence returns to isotropy before entering the second shock, and similarly for proceeding shocks. This latter limit will be denoted as the isotropization case (IC).

In both cases, by assuming sufficiently low-Mach (weak) turbulence, the overall jumps in average background quantities will be approximately unperturbed [43]. Therefore, the overall jump after N shocks can be calculated as the product from each of the single-shock jump relations, given by Rankine-Hugoniot. However, the overall jump of turbulent velocity will depend on whether it returns to isotropy between shocks or not. As such, the two limiting cases will differ.

An idealized, simplified treatment of the IC limit can be achieved by neglecting viscous dissipation during the return to isotropy (this is idealized because the turbulence will experience some decay in energy during the return to isotropy [53]). This is a convenient limit to draw direct comparison to turbulent amplification under an isotropic, uniform (metric) compression. Under the assumption of no viscous dissipation, the overall jump in turbulent amplitude can be calculated in a similar manner to the background quantities, by evaluating the product of the single-shock jumps. For the turbulent velocity, the single-shock jump in amplitude can be calculated using results from LIA, given in Ribner [35]. LIA has been found to agree with direct numerical simulations (DNS) for low mach turbulence [42]. The final turbulent amplification after N shocks can then be calculated from the single-shock jumps

in a similar manner to the background quantities,

$$\frac{A_N}{A_0} = \prod_{i=1}^N \frac{A_i}{A_{i-1}} = \prod_{i=1}^N A_\Delta(m_i), \quad (3)$$

where A_i is the total amplification of a fluid quantity, A , of interest after a number, i , shocks, A_Δ is the individual amplification of A across the i th shock, N is the total number of shocks, and $\rho_\Delta(m_i) = m_i$ by definition.

Generally, however, each shock will introduce some turbulence anisotropy, and the amplification will depend on the turbulent velocity distributions entering each shock. Therefore, in the NIC limit, where turbulence stays anisotropic because of insufficient time to evolve between shocks, the overall amplification cannot be treated as simply. Instead, one can take the results of Ribner's LIA to calculate how the distribution of Kovasnay decomposed vorticity modes is modified by a given shock, which, assuming no nonlinear evolution, is used as the initial condition for the next shock.

For single-shock LIA, the Kovasnay-decomposed vorticity modes of an initially isotropic spectrum of small amplitude, incompressible turbulence are assumed to not interact with each other across the shock. This is satisfied if τ_ϵ is longer than the propagation time through the shock. Linearized inviscid fluid equations and linearized Rankine-Hugoniot relations are used to solve for and relate the perturbations downstream to the upstream conditions for each initial vortical mode. Thus, the problem can be reduced to the interaction of each single vortical mode with the shock, and summed to calculate the overall turbulent amplification. It has been shown that the single-vorticity-mode interactions with a shock can be solved in a two-dimensional (2D) plane containing the mode and oblique shock [32,37], as in Fig. 2 (where we have added an additional shock, to illustrate the extension of the 2D treatment to the multishock case).

The shock has two effects on each vorticity mode: one is a refraction of the mode by shock compression, and the other is an amplification due to both compression and the perturbed, rippled shock front. In Ribner's single-shock calculation, the refracted inclination of a single vorticity mode is given by

$$\tan \theta_1 = m_1 \tan \theta_0, \quad (4)$$

and the energy amplification, S^2 , is calculated as a function of the shock strength and initial vorticity mode inclination in Ref. [34]. Ribner's calculation of S^2 is summarized in the Appendix.

The amplitudes of the downstream longitudinal and lateral components of the turbulent spectrum are calculated in LIA by summing the spectral densities of the refracted, amplified vortices,

$$\begin{aligned} \overline{v_{x1}^2} &= \int |S|^2 \frac{\cos^2 \theta_1}{\cos^2 \theta_0} [\tilde{v}_{x0} \tilde{v}_{x0}] d^3 \mathbf{k}_0 = \int [\tilde{v}_{x1} \tilde{v}_{x1}] d^3 \mathbf{k}_1, \\ \overline{v_{y1}^2} + \overline{v_{z1}^2} &= \int \frac{|S|^2 \sin^2 \theta_1 - \sin^2 \theta_0}{\cos^2 \theta_0} [\tilde{v}_{x0} \tilde{v}_{x0}] d^3 \mathbf{k}_0 + \overline{v_{y0}^2} + \overline{v_{z0}^2}, \end{aligned} \quad (5)$$

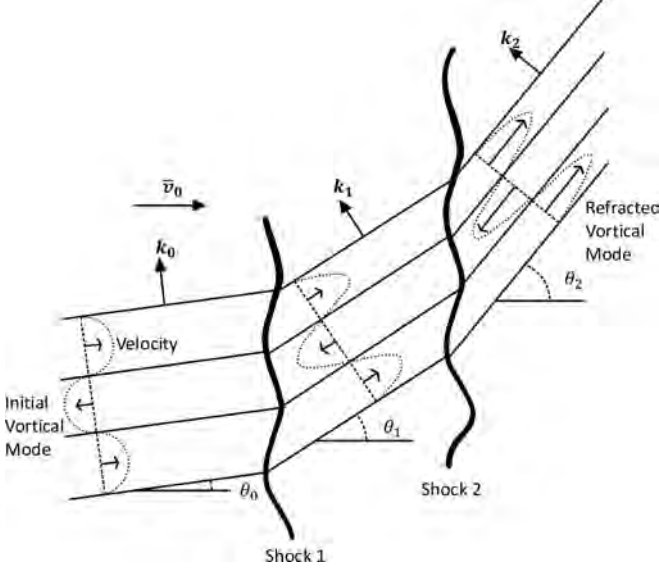


FIG. 2. Refraction and amplification of a vorticity mode convected through two planar shocks on the right. Based on Fig. 3 from Ref. [32], but with entropy and acoustic waves neglected here. The inclination, θ , is defined here as the angle between the velocity perturbations and shock normal (or alternatively, between the wave vector, k , and plane of the shock). This inclination, denoted as θ_i , increases for the refracted wave across each shock.

where \tilde{v}_0 is the turbulent velocity upstream of the shock, \tilde{v}_1 is the downstream turbulent velocity, and $[\tilde{v}_x \tilde{v}_x]$ is the 3D spectral density of \tilde{v}_x^2 in wave-number space.

Since the vorticity mode is only refracted in inclination across the shock and it remains in the same plane, we may assume, using axisymmetry and if there is no evolution, that the 2D treatment still applies for a second shock parallel to the initial shock. Then another refraction and amplification of the mode will occur across the second shock, with S dependent on the strength of the second shock and the refracted inclination of the incoming vortex. This can then be further extrapolated

for N shocks, recursively using the results of Ribner's LIA to calculate the amplitude and inclination of vortices after each shock, and therefore how the longitudinal spectral density changes between shocks,

$$\begin{aligned} [\tilde{v}_{xi} \tilde{v}_{xi}] &= |S_i|^2 \frac{\cos^2 \theta_i}{\cos^2 \theta_{i-1}} [\tilde{v}_{xi-1} \tilde{v}_{xi-1}] \\ &= \frac{\cos^2 \theta_i}{\cos^2 \theta_0} [\tilde{v}_{x0} \tilde{v}_{x0}] \prod_{j=1}^i |S_j|^2, \end{aligned} \quad (7)$$

where $[\tilde{v}_{xi} \tilde{v}_{xi}]$ is the longitudinal spectral density of turbulence downstream of the i^{th} shock, $\tan \theta_i = m_i \tan \theta_{i-1} = \tan \theta_0 \prod_{j=1}^i m_j$ is the vorticity mode inclination after i shocks, and the vorticity mode amplification factor across the i^{th} shock is $S_i = S(m_i, \theta_{i-1})$.

The overall multishock amplification of turbulence can then be calculated from this anisotropic limiting case by summing over the final turbulence spectral densities. For initially isotropic turbulence, $\tilde{v}_{x0}^2 = \tilde{v}_{y0}^2 = \tilde{v}_{z0}^2$, the θ_0 dependency of the initial spectral density is $[\tilde{v}_{x0} \tilde{v}_{x0}](\theta_0) = \cos^2 \theta_0$. Using this with the recursive relation, Eq. (7), one can find the final amplification, after N shocks, of longitudinal and lateral components of initially isotropic turbulence as

$$\frac{\tilde{v}_{xN}^2}{\tilde{v}_{x0}^2} = \frac{3}{2} \int_0^{\pi/2} \cos^2 \theta_N \cos \theta_0 \prod_{i=1}^N |S_i|^2 d\theta_0, \quad (8)$$

$$\begin{aligned} \frac{\tilde{v}_{yN}^2}{\tilde{v}_{y0}^2} &= \frac{\tilde{v}_{zN}^2}{\tilde{v}_{z0}^2} = 1 + \frac{3}{4} \int_0^{\pi/2} \sum_{i=1}^N \frac{|S_i|^2 \sin^2 \theta_i - \sin^2 \theta_{i-1}}{\cos^2 \theta_{i-1}} \\ &\quad \times [\tilde{v}_{xi-1} \tilde{v}_{xi-1}](\theta_0) \cos \theta_0 d\theta_0. \end{aligned} \quad (9)$$

More generally, for initially axisymmetric turbulence, where α is the ratio of the energy in longitudinal modes to the energy in lateral modes such that $\tilde{v}_{x0}^2 = 2\alpha \tilde{v}_{y0}^2 = 2\alpha \tilde{v}_{z0}^2$, the final amplifications of each component after N shocks are given by

$$\frac{\tilde{v}_{xN}^2}{\tilde{v}_{x0}^2} = \frac{\int_0^{\pi/2} \frac{\cos^2 \theta_N}{\cos^2 \theta_0} [\tilde{v}_{x0} \tilde{v}_{x0}] \prod_{i=1}^N |S_i|^2 d\theta_0}{\int_0^{\pi/2} \cos \theta_0 [\tilde{v}_{x0} \tilde{v}_{x0}] d\theta_0}, \quad (10)$$

$$\frac{\tilde{v}_{yN}^2}{\tilde{v}_{y0}^2} = \frac{\tilde{v}_{zN}^2}{\tilde{v}_{z0}^2} = 1 + \frac{\alpha \int_0^{\pi/2} \sum_{i=1}^N \frac{|S_i|^2 \sin^2 \theta_i - \sin^2 \theta_{i-1}}{\cos^2 \theta_{i-1}} [\tilde{v}_{xi-1} \tilde{v}_{xi-1}](\theta_0) \cos \theta_0 d\theta_0}{\int_0^{\pi/2} \cos \theta_0 [\tilde{v}_{x0} \tilde{v}_{x0}] d\theta_0}. \quad (11)$$

We use the amplification calculated by this model for initially isotropic turbulence in both IC and NIC regimes to explore general effects of shock strength and the feedback of generated anisotropy on the multishock compression of turbulence in the next section.

III. RESULTS

A. Trends with shock strength

In some practical situations, such as compression of ICF capsules, there may be a desired final density from shock compression, and the amplitude of any generated turbulence

in the final state may be of interest. To generically understand the influence of shock strength on TKE amplification in the context of multiple shocks in the NIC or IC limits, we first consider a series of N shocks of equal strength. Suppose the final density amplification, ρ_N , is kept fixed, such that the number, N , of identical shocks is determined by the choice of shock strength. The final density amplification is given by Eq. (3) for $A = \rho$ and $m_i = m$ for all shocks, constraining N as

$$N = \frac{\log \rho_N}{\log m}. \quad (12)$$

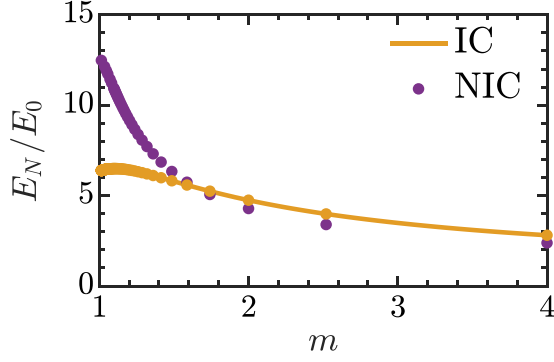


FIG. 3. Final TKE amplification after N shocks of equal strength, m , to reach a final density amplification of $\rho_N/\rho_0 = 16$. The IC limit is shown by the orange points representing integer numbers of shocks, filled in between by an orange line for fractional values of N (physically, the number of shocks must be an integer). The NIC limit is given by the purple points.

Using the definition in Eq. (1) and conservation of mass, the final TKE amplification after N shocks is given by

$$\frac{E_N}{E_0} = \frac{\rho_N}{\rho_0} \frac{V_N}{V_0} \frac{\bar{\tilde{v}}_N^2}{\bar{\tilde{v}}_0^2} = \frac{\bar{\tilde{v}}_N^2}{\bar{\tilde{v}}_0^2}. \quad (13)$$

The volume V_N here refers to the final compressed volume of a characteristic initial volume upstream containing the same perturbations. The details of the volume are unimportant, and V_N is used only to isolate the vorticity amplification from the density compression, i.e., $\rho \propto 1/V$.

First consider the IC limit, where turbulence evolves and returns to isotropy between shocks. Then the final TKE amplification can be found from Eq. (3), for $A = E$, as

$$\frac{E_N}{E_0} = E_\Delta^N, \quad (14)$$

where the amplification across any given shock $E_\Delta(m) = E_i/E_{i-1} = \bar{\tilde{v}}_i^2/\bar{\tilde{v}}_{i-1}^2$ is identical between shocks and can be computed from single-shock LIA via Eqs. (5) and (6).

Substituting for N in Eq. (14) using Eq. (12), E_N can be expressed as

$$\frac{E_N}{E_0} = \left(E_\Delta^{1/\log m}\right)^{\log \rho_N}. \quad (15)$$

In the form of Eq. (15), it is apparent that general trends of how the overall TKE amplification (E_N) depend on single-shock density jumps (m) can be drawn from the bracketed quantity, and the effect of increasing the final density is to magnify any such trends through repeated shocks.

The final TKE amplification for the IC limit as a function of shock strength is given by the orange line in Fig. 3. It reaches a maximum at a shock strength of $m \approx 1.1$, and approaches a minimum towards the strong shock limit. The exact position of this maximum can be determined from Eq. (15) as

$$\frac{dE_N/E_0}{dm} = E_N \ln \rho_N \left(\frac{dE_\Delta/dm}{E_\Delta \ln m} - \frac{\ln E_\Delta}{m(\ln m)^2} \right) = 0, \quad (16)$$

by equating the bracketed quantity to zero. This shock strength for maximally efficient amplification does not depend

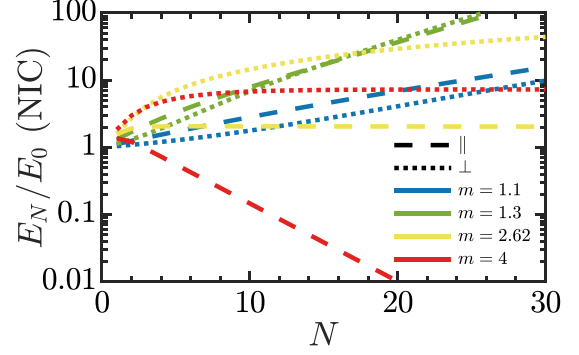


FIG. 4. Total amplification of longitudinal (parallel to shock propagation direction, dashed) and lateral (perpendicular to shock propagation, dotted) components of TKE, in the NIC limit, after launching multiple shocks of strengths (a) 1.1 (blue), (b) 1.3 (green), (c) 2.62 (yellow), (d) 4 (red). Note that different final densities are reached by each strength, for the same number of shocks.

on the final density. Rather, it depends only on what is used for the single-shock TKE jump E_Δ , for which we used Ribner's LIA here [Eqs. (5) and (6)], which itself only depends on γ and m . Thus, for any fixed final density, choosing shocks of strength $m \approx 1.1$ will maximally amplify turbulence for $\gamma = 5/3$ in the IC limit.

Next consider the NIC limit, where turbulence does not return to isotropy. For sufficiently weak turbulence, the jumps in mean background quantities will be unchanged from the IC limit, described by substituting the single-jump Rankine-Hugoniot relations into Eq. (3). However the TKE amplification after N shocks departs from Eq. (3), and is instead given by Eqs. (8) and (9). Therefore, E_N depends on m through the history of how each decomposed vortical mode is amplified at each shock, $S_i(m, \theta_i)$, and refracted, $\tan \theta_i = m^i \tan \theta_0$. Because this differential amplification results in increasingly anisotropic turbulence with each successive shock, the overall amplification E_N also varies nontrivially with the total number of shocks N and final density ρ_N . Regardless, an example for a fixed final density amplification of factor 16 is plotted in purple in Fig. 3. In this NIC limit, the TKE amplification monotonically decreases with increasing shock strength, similar to the isotropic case but without extrema in the trend. Other choices of final density are not shown, however a similar monotonic decrease is observed. For a given final background state in both IC and NIC limits, launching a series of weaker shocks generally results in greater amplification of turbulence than utilizing strong shocks, with the exception of the maximum at $m \approx 1.1$ for the IC limit.

As the turbulence will generally be anisotropic in the NIC limit, it may be instructive to examine the general trends with shock strength for amplification of individual components. This is done in Fig. 4 for launching increasing numbers of identical shocks of strength $m = 1.1$, $m = 1.3$, $m = 2.62$, or $m = 4.0$. $m = 1.3$ is chosen as a relatively weak shock, and because it maintains relative isotropic amplification of both components in the single-shock case. For the series of $m = 1.3$ shocks, the overall amplification stays closer toward isotropy, and monotonically increases with more shocks. The $m = 1.1$ case similarly shows a monotonic increase in

TKE amplification with shock number, albeit preferentially longitudinal and reduced relative to the $m = 1.3$ case for an equivalent number of shocks due to the weaker shock strengths. As the strengths of each shock are increased, the stronger refraction results in preferential lateral amplification over the longitudinal component. After enough shocks, this can result in the amplification of the longitudinal component stagnating, and even being suppressed by additional shocks. This can occur for fewer than 30 shocks if the strength of each shock is greater than $m = 2.61$. The longitudinal amplification for a series of $m = 2.62$ shocks is shown by the yellow dashed line in Fig. 4, which reaches a maximum at 6 shocks, and thereafter the longitudinal amplitude decreases. A more drastic case is shown in red for the strong shock limit, $m = 4$, where the longitudinal component is suppressed strongly by all shocks following the first. In these cases where longitudinal amplification is limited, the ability of shocks to amplify the lateral component reaches a plateau.

B. Polytropic index/quasi-EOS

A more general understanding for how turbulence behaves and partitions energy under compression from multiple shocks can be acquired by constructing a quasi-equation-of-state, similar to Ref. [54], relating TKE to a pressure. From dimensional arguments, this is

$$p_{\text{turb}} \propto \frac{1}{2} \rho \bar{v}^2. \quad (17)$$

This expression for the pressure can then be used to find a polytropic index for the compression of turbulence under a series of shocks:

$$n(N) = \frac{\partial \log p_N}{\partial \log \rho_N}, \quad (18)$$

where $n(N)$ is the polytropic index after N shocks, and p is a pressure that could be thermal or from TKE. Generally, $n(N)$ may depend on the history of compression (the order, number and strength of all shocks up to shock N).

Consider again launching identical shocks of equal strength. In the IC limit, with isotropization between each shock, we can use Eq. (3) for N shocks of strength m , together with Eq. (18) to find the index,

$$n(N) = \frac{\partial \log p_{\Delta}^N}{\partial \log m^N} = \frac{\partial \log p_{\Delta}}{\partial \log m}, \quad (19)$$

which is only a function of the single-shock jumps for density and turbulent pressure. Therefore, by taking a weak-shock expansion of single-shock LIA, one can also find a weak shock limit for the index. We find, to first order in $(m - 1)$, the amplification of the vortical turbulence components in this limit to be

$$\frac{\bar{v}_{xi}^2}{\bar{v}_{xi-1}^2} = 1 + \frac{6}{5}(m - 1) + O[(m - 1)^2], \quad (20)$$

$$\frac{\bar{v}_{yi}^2}{\bar{v}_{yi-1}^2} = \frac{\bar{v}_{zi}^2}{\bar{v}_{zi-1}^2} = 1 + \frac{2}{5}(m - 1) + O[(m - 1)^2]. \quad (21)$$

Combining with Eq. (17) to obtain the vortical turbulent pressure jump, Eq. (19) gives a weak shock index of $n = 5/3$.

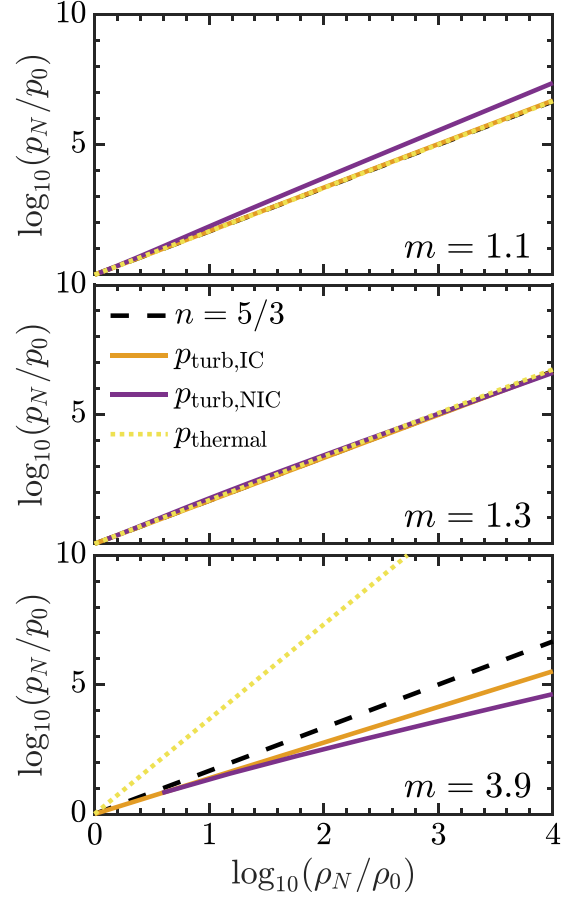


FIG. 5. Total thermal (yellow, dotted) and turbulent (orange for IC, purple for NIC) pressure jumps on a log-log (base 10) scale versus total density jump for multiple equivalent shocks of strengths $m = 1.1$ (top), $m = 1.3$ (middle), and $m = 3.9$ (bottom). Adiabatic prediction of thermal pressure ($n = 5/3$) shown by black dashed line.

A similar weak shock expansion of the thermal pressure also yields the same polytropic index of $n = 5/3$, corresponding to the adiabatic limit.

As has been discussed in the previous section, due to the feedback of anisotropy, the amplification of TKE across any given shock in the NIC limit depends nontrivially on previous shocks. Therefore, the NIC polytropic index is also a function of the history of shocks. The instantaneous value of n for a given shock in a series can be inferred from the TKE amplification by taking the gradient of the curves in Fig. 5, which shows $\log(p_N/p_0)$ plotted against $\log(\rho_N/\rho_0)$ for increasing numbers of shocks, N , of strengths $m = 1.1$, $m = 1.3$, $m = 3.9$ in both the NIC and IC limits.

Inspection of the gradients for the IC limit with $m = 1.1$ and $m = 1.3$ in Fig. 5 reveals that the weak-shock IC limit tends towards an index of $n = 5/3$, as predicted from the weak-shock expansion of LIA. Therefore, in the limit of shocks being sufficiently weak and isotropization between shocks (IC), a compression via repeated shocks corresponds to a 3D, isotropic, adiabatic metric compression. Curiously, the NIC limit with $m = 1.3$ also shows an index close to $n = 5/3$, owing to the relative isotropy of amplification predicted by LIA in this case, even with repeated shocks, as seen in Fig. 4.

However, conversely, the weak-shock NIC limit exhibits a steeper slope, with a superadiabatic index $n \approx 1.83 > 5/3$, requiring more energy to compress.

Increasing the shock strength results in a greater proportion of heating than compared to compression and turbulence amplification. This is perhaps expected from single-shock jump trends, where the density and TKE jumps are bounded, whereas the temperature jump is unbounded in the strong shock limit. We see this manifesting in the IC and NIC effective indices in Fig. 5, where the index for the turbulent pressure decreases with shock strength, while that of the temperature can increase unbounded in the strong shock limit. Thus, in the strong shock limit nearly all the compression energy does work against the thermal pressure and goes into heating. The effects of increasing shock strength are more adverse in the NIC limit, where the TKE amplification can become highly anisotropic when strong shocks are launched repeatedly, as in Fig. 4. The effect of this increasing anisotropy on the instantaneous index can be inferred from the purple line in Fig. 5, whose gradient decreases with an increasing number of shocks in the strong-shock case. As in Fig. 3, a series of stronger shocks does not amplify TKE as efficiently, and so the strong-shock index decreases as the turbulence becomes increasingly anisotropic with each shock, such that minimal work is done against TKE by the compression.

C. Shock ordering

In some compression scenarios, such as achieving a low adiabat in ICF, multiple shocks of different strengths may be used and the order selected to minimize the required energy or to ensure stability [7]. Imagine such a scenario with a desired compression level after multiple shocks (as previously considered in Sec. III A) but now with shocks of possibly unequal strength. Because the final compression is fixed, the mean quantities again do not depend on the shock order. However, given the previous discussion on the dependence of TKE amplification in the NIC limit on the history of shocks, the amplification of turbulence may be sensitive to a change in the order in which the shocks are launched.

The top panel of Fig. 6 shows a contour plot of the the amplification of TKE after a shock of strength m_1 (horizontal axis), followed by a shock of strength m_2 (vertical axis), for initially isotropic turbulence in the NIC limit. The amplification is asymmetric between the two shocks. This can be seen from the shapes of the contours or following a path of constant final density (e.g., $m_1 m_2 = 6$), along which E_2/E_0 is seen to be greater for the half of the path at $m_1 < m_2$. Furthermore, TKE amplification reaches a maximal value of $E_2/E_0 = 2.5$ for shocks of strengths $m_1 = 2.7$ and $m_2 = 3.4$, but reversing the order of shocks such that $m_1 = 3.4$ and $m_2 = 2.7$ reduces the amplification to $E_2/E_0 = 2.43$.

This asymmetry in TKE amplification with respect to shock order is more apparent from calculating an ordering ratio, R , of the amplification with one ordering of shocks versus the other,

$$R(m_1, m_2) = \frac{E(m_1, m_2)}{E(m_2, m_1)}, \quad (22)$$

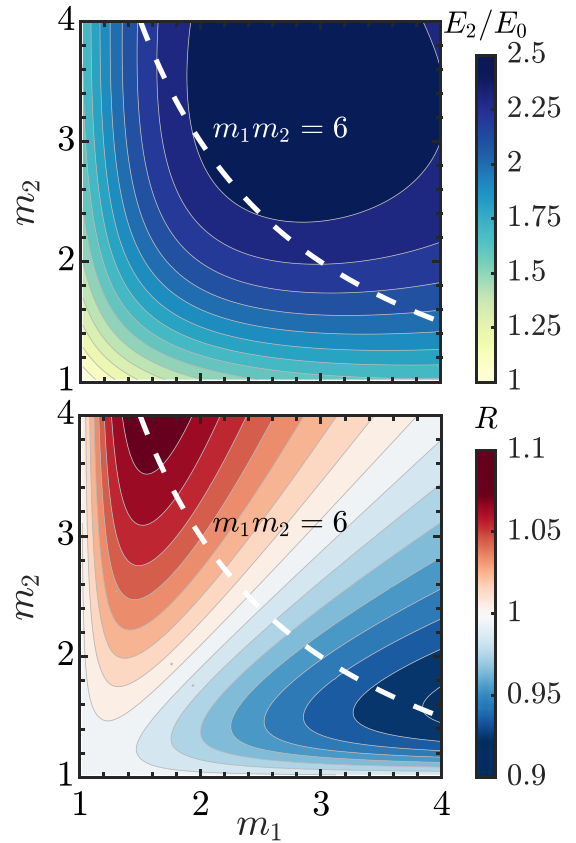


FIG. 6. Top: Contour plot of TKE amplification, after two shocks, E_2/E_0 , for an initially isotropic distribution of turbulence, in the NIC limit. Strength of initial shock is given on the horizontal axis, and of the second shock on the vertical axis. Bottom: Corresponding contour plot of ordering ratio, R . The maximal difference is a factor of 1.084 for an initial weaker shock of $m = 1.58$, followed by a strong shock of $m = 4$. An example contour of constant final density amplification of factor 6 is shown by the white dashed line in both plots.

where $E(m_1, m_2)$ is the amplification of TKE after a shock of strength m_1 , followed by m_2 . Values of $R > 1$ mean the original ordering of shocks leads to greater amplification than if the order was reversed.

The ordering ratio, R , corresponding to the TKE amplification example in the top panel of Fig. 6, is similarly plotted against m_1 and m_2 in the bottom panel of Fig. 6. As expected, R is “antisymmetric” around the diagonal, $m_1 = m_2$, in the sense that $R(m_1, m_2) = 1/R(m_2, m_1)$. That the plot is red in the upper diagonal and blue in the lower diagonal shows that $R > 1$ for $m_1 < m_2$, and $R < 1$ for $m_1 > m_2$. Therefore, for two given shock strengths, the TKE amplification of initially isotropic turbulence by the two shocks is maximized if the weaker shock is launched first.

The maximal difference in amplification due to shock ordering is a factor of $R_{\max} = 1.084$, if the order of two shocks of strength $m = 1.58$ and $m = 4$ are swapped. While $R_{\max} = 1.084$ may be small for the isotropic distribution of turbulence, turbulence in experiments and nature can often be highly anisotropic and the difference in amplification due to shock order can potentially be enhanced. To understand this

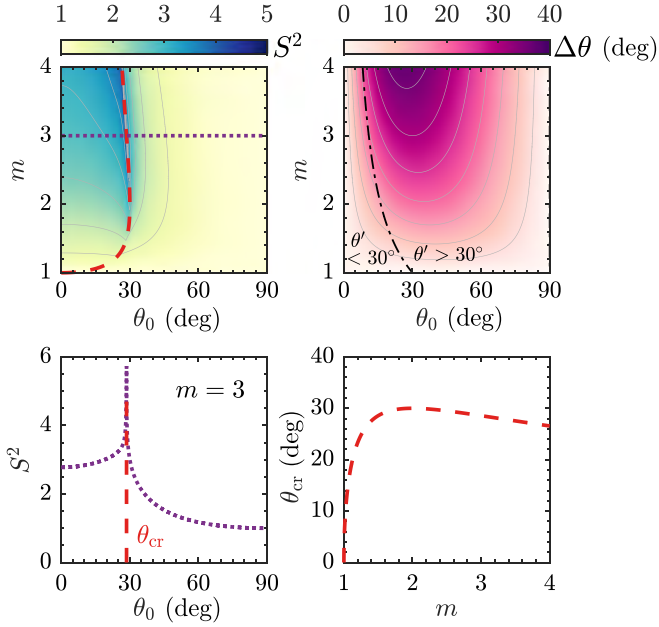


FIG. 7. Top: 2D plots of amplification of energy (S^2 , top left) and refraction (change in inclination, $\Delta\theta = \theta' - \theta_0$, top right) of a single vortical mode of initial inclination θ_0 , by a single shock of strength m . Isocontours of the respective quantities are also plotted. The dash-dotted black line (top right) is the isocontour for $\theta' = \theta_{cr} = 30^\circ$. To the right of this isocontour, the refracted mode will exceed the critical inclination for any additional shocks. Bottom left: Amplification of vortical mode energy by a single shock of strength, $m = 3$ (path along purple dotted line in top plot), plotted against initial inclination of the vortical mode. A vertical red dashed line is plotted at the critical inclination for $m = 3$, $\theta_{cr} = 28.56^\circ$. Bottom right: Critical initial inclination, θ_{cr} , of a vortical mode for a shock of strength m . This is also plotted by the red dashed line in the top left panel.

and as a general approach, it is important to examine how the sensitivity to shock order for individual vortical modes can be much greater for certain initial inclinations.

The LIA dependence of the single-shock energy amplification of an individual vortical mode on its inclination is shown in the left panels of Fig. 7, which plot S^2 against initial vortical mode inclination θ_0 and shock strength m (top left), and versus θ_0 for a fixed $m = 3$ (bottom left). There exists a sharp peak in amplification at a “critical inclination,”

$$\theta_{cr} = \arctan \sqrt{\frac{(\gamma + 1)(m - 1)}{2m^2}}, \quad (23)$$

for which the resultant postshock flow in the steady-flow frame (transformation velocity increases with inclination) reaches the sound speed [35]. At θ_{cr} , the amplification in vortical mode energy can be several times larger than at the smallest inclinations. This finite peak can be seen in the $m = 3$ example, where $\theta_{cr} = 28.56^\circ$. With increasingly transverse inclinations beyond the critical inclination, the amplification is rapidly suppressed. While the critical inclination of a vortical mode depends on the strength of the shock, as plotted for Eq. (23) in the bottom right panel of Fig. 7, it is generally a preferentially longitudinal inclination that reaches a maximum $\theta_{cr, \max} = 30^\circ$ for a shock of strength $m = 2$ and

$\gamma = 5/3$. For a large range of shock strengths above $m = 1.126$, θ_{cr} lies between $20^\circ < \theta_{cr} < 30^\circ$.

The corresponding refraction of a vortical mode of inclination θ_0 through a single shock of strength m is given by the change in its inclination, $\Delta\theta$, plotted in the top right panel of Fig. 7. This refraction is greater for stronger shocks, predominantly for intermediate inclinations around typical θ_{cr} . The black dash-dotted line separates the plot into a region where the postshock inclination, $\theta' = \Delta\theta + \theta_0$, is below the maximum critical inclination, $\theta' < \theta_{cr, \max}$ (left of the line), or exceeds the maximum $\theta' > \theta_{cr, \max}$ (right of the line). This left region demarcates the parameter space of initial vortex inclination and initial shock strength for which the refracted vortical mode could still experience critical effects for subsequent shocks.

We now consider such a two-shock system, where the strengths of each shock are denoted by m_1 and m_2 , and we can choose to launch either m_1 or m_2 first, followed by the remaining shock. We will denote the initial inclination of the vortical mode to be θ and the inclination after the first shock to be θ' . Then θ' will depend on which of the shocks is launched first, $\theta'(m_i, \theta) = \arctan[m_i \tan(\theta)]$. The two-shock energy amplification is given by the product of the amplifications from each shock, which depend on the incoming vortical mode inclinations and individual shock strengths, $S_{12}^2 = S^2(m_1, \theta)S^2(m_2, \theta'(m_1, \theta))$. If the order of the shocks is reversed, then $S_{21}^2 = S^2(m_2, \theta)S^2(m_1, \theta'(m_2, \theta))$. The ordering ratios for a single vortical mode, $R(m_1, m_2, \theta) = S_{12}^2(\theta)/S_{21}^2(\theta)$, therefore expresses the difference in amplification of vortical-mode energy due to shock ordering.

If the initial vortical mode inclination is too longitudinal with respect to the shock, then the vortical mode cannot be refracted enough to reach the range of critical inclinations shown in the bottom right panel of Fig. 7 for the second shock. For example, vortical modes with $\theta_0 \approx 0$ (top right panel) are not refracted to the $20^\circ < \theta' < 30^\circ$ range. Likewise, if the initial inclination surpasses 30° ($\theta > \theta_{cr, \max}$), then it is beyond the critical inclination for both of the shocks.

Ordering ratios for inclinations far outside the range of criticality, such as $3^\circ \ll \theta_{cr}$ and $60^\circ \gg \theta_{cr}$, are plotted against m_1 and m_2 in the top panels of Fig. 8. In the far-subcritical regime ($\theta \ll 20^\circ$, e.g., 3°), the amplification is maximized with a stronger initial shock that refracts the vortical mode more strongly to (still subcritical) inclinations where the subsequent shock amplification is slightly increased. For example, at $\theta = 3^\circ$, amplification is slightly enhanced by up to a maximum of 0.58% for $m_1 = 4$ and $m_2 = 1.6$. In the supercritical regime ($\theta \gg 30^\circ$, e.g., 60°), the amplification is instead maximized by launching the weaker shock first to minimize refraction such that the inclination of the vortical mode does not depart as far from θ_{cr} for the subsequent shock. For $\theta = 60^\circ$, amplification can be up to a maximum of 8.26% greater for $m_1 = 1.93$ and $m_2 = 4$. In both of these noncritical regimes, because the amplification is not greatly enhanced by critical effects for either shock, the differences in TKE amplification due to shock ordering are minimal.

Conversely, closer to the range of critical angles ($\theta \lesssim 30^\circ$), differences in amplification due to ordering can be substantially larger. Amplification of vortical mode energy at example inclinations of $15^\circ < \theta_{cr}$ and $30^\circ = \theta_{cr, \max}$ is plotted in the

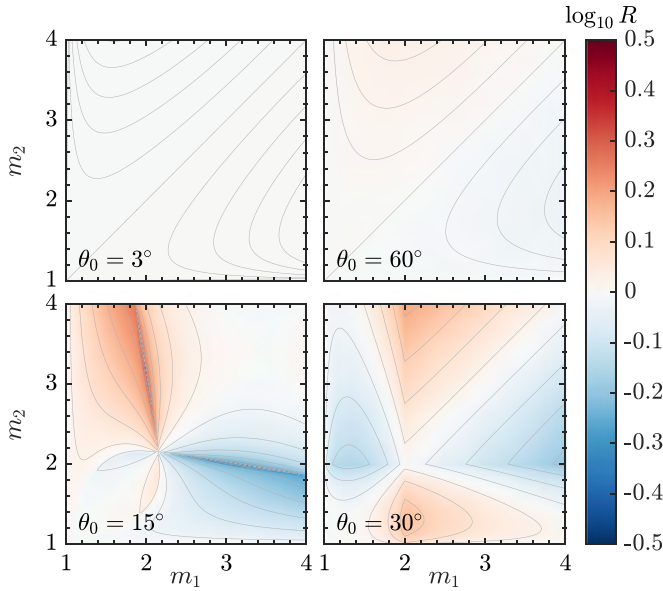


FIG. 8. 2D logarithmic (base 10) plots of ordering ratio R , for the two-shock amplification of vortical modes of varying initial inclination between each subplot (3° , 60° , 15° , and 30°), in the NIC limit. Strength of initial shock is given on the x axis, and of the second shock on the y axis. Isocontours of $\log R$ are overlaid.

bottom panels of Fig. 8. In the near-subcritical regime ($\theta \lesssim 20^\circ$), a weaker first shock can refract the vortical mode to inclinations that are critical for a stronger second shock, maximizing the amplification substantially compared to the reverse configuration that greatly minimizes the amplification. An example of this is shown for an initial inclination of 15° in the bottom left panel of Fig. 8. Most of the space for $m_1 < m_2$ results in values of $R > 1$, with a maximum of $R = 3.19$: a factor 3.19 greater energy amplification for a vortical mode, initially inclined at 15° , can be achieved by launching a weaker shock of strength $m_1 = 1.94$ followed by a shock of strength $m_2 = 3.54$ than if the shocks were reversed in order.

For inclinations close to the maximum critical inclination $\theta \approx 30^\circ$, refraction by even relatively weak shocks (see Fig. 7, top right) will result in a supercritical inclination for a following stronger shock and suppress the overall amplification. Therefore, in this regime, the amplification can instead be maximised by choosing the strength of the first shock such that the initial inclination is critical, regardless of the strength of the second shock. Reversing the order of the shocks, such that the first noncritical shock refracts the initial vortical mode beyond the critical inclination of the other shock, will not produce as large an amplification. An example of this regime is shown for $\theta = 30^\circ$ in the bottom right panel of Fig. 8. An inclination of $\theta = 30^\circ$ is critical for a shock of strength $m = 2$. Therefore, the amplification when launching a critical first shock of $m_1 = 2$ followed by a strong shock of $m_2 = 4$ is 54.1% greater than launching a first shock of $m_1 = 4$ followed by $m_2 = 2$.

We therefore see for these inclinations where critical angle effects come into play in the multishock problem, the differences in vortical mode amplification are substantially more extreme, with over a factor of three difference being possible

for an initial inclination of 15° . This is in stark contrast to the few percent differences observable for inclinations far from critical angle effects, and for an initially isotropic distribution of turbulence. For the latter case, the large differences due to near-critical vortical mode components of the turbulence are smoothed out by the other far-critical components.

IV. DISCUSSION

We now discuss the relevancy of the significant findings for certain example applications. It was mentioned and explored in Sec. III A (particularly in Fig. 3) that for certain scenarios, such as in ICF, the final density from shock compression may be fixed, and the amplitude of turbulence in the final state could be of interest.

There could be scenarios where a final state with maximal turbulence is desired, for example a fast ignition scheme where compression energy can be transferred to TKE and released in a final compressed state [55]. In a variation of such a fast ignition scheme, the TKE may in and of itself be advantageous to directly increase the hot spot fusion reactivity [56]. In such a setup, our analysis has shown launching a series of weaker shocks to be optimal for TKE amplification, especially so for the NIC limit. This is generally true in the IC limit too, albeit with shocks of strength $m = 1.1$ being optimal for $\gamma = 5/3$. A series of weaker shocks also has the benefit of minimizing the proportion of compression energy used on heating, with both turbulent and thermal pressures exhibiting adiabatic behavior in the weak-shock limit.

However, if turbulence in the final state needs to be minimized such as to reduce mix, then a series of fewer, stronger shocks should be chosen, for the same final compression. This is particularly the case for the NIC limit, which also has the additional effect of magnifying the turbulent anisotropy. This anisotropy reduces further amplification and favors components of turbulence transverse to the shock while suppressing the longitudinal components. Therefore, in this limit for an ICF capsule, the longitudinal turbulent fluctuations will be suppressed by a series of strong shocks, further reducing mixing in the radial direction and associated cooling of the hotspot. However, these turbulence considerations of course need to be balanced against the other design constraints, since stronger shocks result in a greater proportion of heating.

The most major difference from the IC limit is the effect of shock ordering in the NIC limit. We have shown how while background mean quantities are agnostic to the order of shocks for weak turbulence, the TKE amplification can be sensitive to shock order. This sensitivity to shock ordering may be an additional factor to consider when choosing shocks in compression scenarios such as ICF.

For just the two-shock case with initially isotropic turbulence, differences of up to only 8.4% are possible from swapping the order of the two shocks, with the larger turbulence amplifications coming from launching the weaker shock first. Such differences could be changed with the addition of more shocks, or with different initially anisotropic distributions of turbulence that are often more physically common than the ideal case of isotropic turbulence. We have shown how this can be done for the two-shock case with individual

vortical modes. The sensitivity to shock ordering strongly depends on the initial inclination of the vortical mode with respect to the shock, with up to a factor 3.2 difference in TKE amplification for an inclination of 15° .

Alternatively, this sensitivity presents a novel diagnostic for shock ordering. One could imagine a situation where there exists an anisotropic distribution of turbulence consisting mainly of vortical modes within a range of near-critical inclinations. It would then be expected that if it were to be passed through two shocks, one with $m_1 \approx 2$ and $m_2 \approx 4$, and then again with the orders reversed, one could determine the order in which they were launched based on the turbulent amplification. This would typically be difficult to determine from comparing the mean quantities in the initial and final states.

In general the small scale dynamics of ICF implosions (in particular mixing between materials, as might be influenced by differences in TKE from shock ordering) are challenging to diagnose directly, although if the differences lead to differences in mixing behavior, then those differences might be diagnosed (e.g., Refs. [57–59]). Laser interferometry has been used in the past to diagnose differences in the perturbed shock dynamics for shocks that pass through various ablator materials and into a witness material [60]. This diagnostic is quite sensitive at detecting perturbations to the shock front that represent small fractional changes from the mean shock velocity; these shock front perturbations are related to the postshock perturbations, and so this might be another route by which to attempt to diagnose the differences discussed in this work.

While the results presented in Sec. III assume initially isotropic turbulence, the consequences of feedback of generated anisotropy in the NIC limit provides an intuition on how our other results would change for initially anisotropic turbulence. For example, from the discussion on Fig. 4 and the enhanced amplification of subcritical vortical modes seen in Fig. 7, turbulence that consists of dominantly longitudinally oriented vortical modes could be expected to be amplified more strongly than isotropic turbulence.

This type of axisymmetric turbulence is naturally generated in simulations of ICF implosions including perturbation sources, such as in the first NIF experiment to achieve an igniting fusion plasma [13,61,62]. There are three shocks in this experimental design. In 2D simulations including initial density perturbations in the ablator from its grain structure [17], the first shock (strength $m_0 \approx 2$) generates an initial vorticity field which is strongly biased towards perturbations that are longitudinal relative to the second and third shocks of strengths $m_1 \approx 1.75$ and $m_2 \approx 2$, respectively.

Taking the postshock vorticity spectrum as a function of inclination from the simulation in Ref. [17], and assuming, given axisymmetry, an equal partition between energy in longitudinal and lateral modes in 3D as was in the 2D simulation, multishock amplifications of this initially axisymmetric turbulence can be calculated using Eqs. (10) and (11). For the whole shock-strength parameter space, we find the maximum TKE amplification to be $E_2/E_0 = 7.97$ (for $m_1 = 3.8$ and $m_2 = 4$) in the NIC limit, over three times greater than the maximum amplification of $E_2/E_0 = 2.50$ available to initially isotropic turbulence. We predict the amplification of TKE after shocks

$m_1 = 1.75$ and $m_2 = 2$ from the experimental design to be a factor of $E_2/E_0 = 4.60$. For initially isotropic turbulence, we find amplification factors of $E_2/E_0 = 2.11$ in the NIC limit, and $E_2/E_0 = 2.06$ in the IC limit. Therefore, we predict the expected amplification in this design to be twice as large for this example of realistic turbulence with a longitudinal bias than for isotropic turbulence, consistent with expectations from our results. For an initial turbulent velocity of ~ 0.5 km/s from Ref. [17], we expect a final turbulent velocity of $\sim 0.5\sqrt{4.6} = 1.07$ km/s.

For small scale perturbations generated in the ablator of an ICF implosion in response to the sequence of shocks, as in Ref. [17], the Mach number of the perturbations is expected to be very small, because only a modest fraction of the energy in the postshock state is converted to perturbations. This is the applicable limit for the scenario we examined above, where simulations suggest $M_t \lesssim 0.03$. Nonetheless these small perturbed velocities (relative to the implosion velocity) can have a notable impact by contributing to mixing of ablator layers (see, e.g., Fig. 11 in Ref. [63] and the surrounding discussion), or to mixing of the ablator with the fusion fuel [17,63]. For perturbations in the central hot spot of the implosions, higher (but still well subsonic) turbulent Mach numbers have been observed in modeling. For example, Ref. [64] estimates $M_t \sim 0.4$ for the hot-spot turbulence observed in the 3D simulations of a NIF implosion in Ref. [65]. Although the shock dynamics in the hot spot are not identical to those in the ablator, this hot spot turbulence is again influenced by a succession of shocks (e.g., see Fig. 1 in Ref. [65]).

The predicted ideal jumps in background density and temperature (ignoring rarefactions between shocks that occur in the actual ICF design) under these two shocks are $\rho_2/\rho_0 = 3.5$ and $T_2/T_0 = 3.68$, both less than the energy amplification of the anisotropic turbulence. From our quasi-EOS analysis in Sec. IIIB, this indicates that this anisotropic turbulent pressure would behave superadiabatically under compression for this experiment, more so than the thermal pressure. Since the turbulence is more anisotropically biased in the direction of shock compression, more work needs to be done against the turbulent pressure.

The difference in amplification under swapping the order of the two shocks is relatively negligible for this anisotropic distribution of turbulence, only 1.10%, less than the difference of 1.33% for isotropic turbulence. Even for unconstrained choices of shock strength, the maximal factor difference due to ordering is only $R_{\max} = 1.062$ (6.2%), less than the $R_{\max} = 1.084$ (8.4%) of isotropic turbulence. Since most of the energy in vorticity generated by these grains is in far-subcritical vortical modes with inclination $\theta < 10^\circ$, critical angle effects are negligible for the two proceeding shocks. This could change, however, if there was an additional shock to further refract these modes to near-subcritical inclinations. Suppose the turbulence is subjected to an initial shock of $m_1 = 2.2$, and the strengths of two proceeding shocks are chosen as m_2 and m_3 . For the axisymmetric turbulence from the grain simulation, a maximal difference of factor $R_{\max} = 1.128$ is possible upon swapping two shocks of strengths $m_2 = 1.54$ and $m_3 = 4$. This is a greater difference than for initially isotropic turbulence in the two-shock problem and also in this three-shock problem where $R_{\max} = 1.110$.

Both the NIC and IC limiting cases we studied in Sec. III are only applicable when the time separation between shocks is sufficiently shorter or longer than the timescale over which turbulence returns to isotropy after each shock. Direct numerical simulations have shown the vorticity returns to isotropy after ten convected Kolmogorov timescales, $\tau_\eta = \sqrt{\nu/\epsilon}$, where ν is the kinematic viscosity and ϵ the dissipation rate of turbulent kinetic energy [48]. However, the turbulent velocity was found to remain anisotropic in their simulated domains, and one might expect a return to isotropy over a longer distance away from the shock. Provided this distance is greater than the necessary shock separation to avoid overtaking of shocks, the first limiting case can be achieved with minimum shock separation. The second case is possible by making the shock separations longer than both the required shock separation and the distance needed for return to isotropy; with the caveat that if the separations are too great, then nonnegligible viscous dissipation and nonlinear effects can occur that we have neglected in this model.

However, even for situations in between the two cases, where the turbulence begins an incomplete return to isotropy before the next shock, one may anticipate results to be a mix of the two limiting cases. For example, shock ordering does not matter for the isotropized case, while TKE amplification in the NIC limit is sensitive to it. One may expect for realistic regimes in between these two cases, that shock ordering differences in TKE amplification will still manifest, but to a lesser degree.

To model such scenarios, where turbulence evolution is important, is outside the scope of this work. Such evolution may be governed by nonlinear processes not included in LIA [45] and require the inclusion of viscous dissipation.

Further, any caveats of LIA will also appear in our model, even for the two limiting cases. We have assumed weak turbulence to use LIA, and to treat the jumps in background quantities as unperturbed from classical Rankine-Hugoniot shock-jump relations for density, temperature and mean flow speed. Under continuous amplification by many shocks, the turbulence could eventually become energetic enough relative to the shocks, that this assumption is broken. In DNS, disagreement with LIA in TKE amplification and mean Rankine-Hugoniot jumps is found for higher turbulent Mach numbers. However, there have been more recent theories that treat finite Mach turbulence and the modifications to jumps in background quantities [43], that could also be adapted similarly for our model here. Moreover, the velocity anisotropies in DNS are observed to be different from the predictions of LIA [45], which would alter the NIC limit.

Here we have only taken the vortical contributions to turbulence in calculating amplifications. However, there is also an acoustic pressure contribution to the downstream waves that we have neglected which is also computed in Ref. [34]. For a vorticity mode that is incident at a subcritical angle $\theta < \theta_{cr}$ on a planar shock, the downstream pressure waves are evanescent and exponentially decay with distance from the shock front. When the incident vorticity mode exceeds θ_{cr} , constant amplitude sound waves are spontaneously generated at the shock front and propagate away at an angle relative to the downstream vorticity mode. The amplitude of these sound waves has a finite maximum at θ_{cr} and decreases with increas-

ing inclination of the incident vorticity mode [34,38]. The spontaneous generation of noise by a rippled shock front is a general phenomenon also described in Chap. 90 of Ref. [66]. For the case of incident sound waves, there exists a critical inclination at which they experience a resonance and linear analysis breaks down [67,68]. When higher order terms are included, the amplification of these sound waves remains enhanced, but finite [69].

For most shock strengths, acoustic generation is of a few percent relative to that of the initial vorticity mode, and so our analysis should be a reasonable approximation for fewer numbers of shocks. Compared to the amplification of the vorticity, however, the noise generation can be more efficient in the weak shock limit [37], particularly for critical inclinations of the initial vorticity mode, as mentioned above. Furthermore, these sound waves can be greatly amplified by subsequent stronger shocks if they are critically inclined [69].

For our analysis with initially isotropic vortical turbulence, the generated noise will be distributed over a wide variety of inclinations, and so subsequent amplification and generation of sound waves would likely only perturb our analysis for a sequence of a large number of shocks. Likewise, for our analysis of shock ordering, only two to three total shocks are considered. While we consider distributions of vorticity modes near the critical angle in some of this analysis, the generated acoustic waves downstream of the first shock will generally be weak relative to the energy of the initial vorticity mode. As such, the perturbation to the second shock and vorticity amplification may not be a large effect, even at the critical inclination. Moreover, sound waves that are critical with respect to the second shock may not necessarily remain critical for the third shock and the shocks after.

Regardless, for large numbers of shocks where generated noise can reach an appreciable amplitude, our analysis should be extended to include the acoustic contribution.

In addition, our work neglects the effects of density nonuniformity, which has been shown to be important for turbulence generation by shocks in certain contexts such as the aforementioned examples of grain structure in ICF ablaters [17,18]. However, thermal conduction in such cases can smooth the postshock density field, so that any subsequent shocks following the first would primarily interact with the vorticity field.

The analysis presented in this paper restricts attention to only hydrodynamic turbulence. While ablator and dense fuel dynamics in ICF are generally well treated by such a model, magnetic fields could play a role in the central hot spot [70,71]. Furthermore, there are a plethora of other regimes of interest where magnetohydrodynamic (MHD) turbulence can interact with shocks, for example with interplanetary shocks due to multiple solar flares. While the solar wind is a weakly collisional plasma, and kinetic effects can be important for small-scale processes such as ion heating [72], nonlinear relaxation processes can reduce the effective mean free path of protons and enable the solar wind to behave like a magnetised fluid on scales above the proton gyroradius [73]. Thus, with a plethora of *in situ* spacecraft measurements [74], the solar wind could be particularly well suited for testing theories of the interaction of MHD turbulence with shocks. The multi-shock amplification of MHD turbulence would be a natural

extension of our theory in future work, using linear analyses of the single-shock problem, such as in Refs. [75,76].

V. CONCLUSION

We use a linear analytical model following the single-shock results (LIA) of Ribner [35] to study the interaction of an incompressible, isotropic spectrum of turbulence with multiple planar shocks in two limits: (1) the turbulence fully returns to isotropy between each shock (IC limit), or (2) shocks occur rapidly in time such that the turbulence spectrum does not evolve between shocks (NIC limit). We assume the jumps in background quantities are unperturbed for sufficiently weak turbulence. For a variety of number and strengths of shocks, we examine the amplification of vortical turbulent kinetic energy (TKE) across multiple shocks, opting to neglect the acoustic contribution. By extracting the effective polytropic indices for the turbulent pressure amplification, we infer general properties of the multishock compression of turbulence. To further inform the sensitivity to shock ordering in the NIC limit, we also consider the multishock interaction with single vorticity modes for certain example inclinations with respect to the initial shock.

We find that choosing to launch a greater number of weaker shocks to reach a fixed final background state will generally result in greater amplification of turbulence than a series of fewer stronger shocks. In particular, in the IC limit, we find maximal TKE amplification (without regard to relative temperature amplification) for a series of weak shocks with strength $m \approx 1.1$. As shock strength tends towards unity for this IC limit, we infer the polytropic index to be $5/3$, revealing that an arbitrarily weak multishock compression of turbulent pressure is equivalent to that of an isotropic, adiabatic volumetric compression. In the NIC limit of many weak shocks, the polytropic index is instead superadiabatic, for example $n \approx 1.83$ for $m = 1.1$. As the multishock amplification of turbulence becomes less efficient towards greater strength shocks, the associated polytropic index decreases for both IC and NIC limits, with the latter becoming adiabatic, $n = 5/3$, at $m = 1.3$. The polytropic index of the temperature instead increases with shock strength, and so stronger shocks convert a greater proportion of energy into heating than into compression and turbulent amplification.

We show how the anisotropy in the NIC limit affects the multishock amplification of turbulence, both in its components relative to the shock fronts and overall. Stronger shocks magnify the anisotropy, accelerating the departure of the NIC limit from the IC limit by reducing TKE amplification and its polytropic index with respect to multishock compression, as the number of shocks increases. Therefore, the polytropic index associated with the NIC limit is generally dependent on the shock history.

In addition for the NIC limit, TKE amplification is sensitive to not only the choice of shock strengths, but the order in which each shock is launched. With two shocks, for example, differences in amplification of up to 8.4% are possible for initially isotropic turbulence, when the two shocks are switched in order. Single vortical modes can exhibit far greater sensitivity to ordering when the vortical mode inclination is within a band below the critical angle, with up to 219% amplification

difference upon swapping two shocks of strengths $m = 1.94$ and $m = 3.54$ for an example initial inclination of 15° . It is therefore likely that certain anisotropic spectra of turbulence can be highly sensitive to the ordering of certain strength shocks.

Our use of LIA to examine multishock compression of turbulence in two limits informs a simple intuition for how turbulence may behave under multishock compression and the impact of shock strengths. We reveal an interesting sensitivity of TKE amplification to the order in a choice of strengths of shocks. While one could intuit behavior in a regime between the two limits, further work on a model that includes the evolution of the turbulence spectrum in between shocks, with viscous dissipation, remains to be explored. Future extension to linear analyses of MHD shock-turbulence interaction would also expand the applicability of the theory to a wider variety of plasma regimes.

ACKNOWLEDGMENTS

This work benefited from useful conversations with Christopher Weber. M.F.Z. and N.J.F. acknowledge support, in part, from Department of Energy Grant No. DE-AC02-09CH1146 and by the Center for Magnetic Acceleration, Compression, and Heating (MACH), part of the U.S. DOE-NNSA Stewardship Science Academic Alliances Program under Cooperative Agreement No. DE-NA0004148. M.F.Z. acknowledges support from the Defense Science and Technology Internship program at LLNL. This work was performed under the auspices of the U.S. Department of Energy by the Lawrence Livermore National Laboratory under Contract No. DE-AC52-07NA27344. S.D. was supported by the LLNL-LDRD Program under Project No. 20-ERD-058.

DATA AVAILABILITY

The data that support the findings of this article are not publicly available. The data are available from the authors upon reasonable request.

APPENDIX: SINGLE-SHOCK AMPLIFICATION OF A SINGLE VORTICAL MODE

Presented is a summary of Ribner's calculation of S^2 [34], the energy amplification of a single, inclined vorticity mode upon convection through a planar shock. The amplitude of the initial vorticity mode is assumed to be weak, such that perturbations to the mean flow are small.

Schematically, the convection of the initial vorticity mode through a normal shock can be visualized by only considering the first shock in Fig. 2. The troughs and peaks of the inclined vorticity mode will travel vertically along the shock front in time, which propagates a ripple perturbation along the shock front. For a general plane vorticity mode, the shock front develops ripples in a 2D plane. However, since the out-of-plane component of the vorticity mode would be parallel to the plane of the rippled shock-wave, the third dimension plays no role and the problem can be treated two-dimensionally.

The time-dependence of the problem can be removed by transforming to a frame where the bulk flow is aligned with

the perturbed velocity of the vorticity mode. See Figs. 3 and 4 of Ribner [34], where a velocity transformation, V , parallel to the shock front, is taken. The mean velocity of the upstream (downstream) flow in the transformed frame is then \bar{W}_0 (\bar{W}_1), and the Mach speed of this flow is denoted by \bar{M}_0 (\bar{M}_1). For initial vorticity modes with higher inclination, V will be greater, and the mean flow in the transformed frame becomes more oblique relative to the shock.

In this time-independent steady-flow frame, the calculation is reduced to a boundary-value problem. To derive a partial differential equation describing this flow, consider axes ξ and η aligned parallel and perpendicular, respectively, to the mean downstream flow, \bar{W}_1 . These axes are illustrated in Fig. 4 of Ribner [34].

Assume the initial vorticity mode is weak such that the perturbations to the mean flow \tilde{v}/W are small, and the background density, temperature, and pressure remain approximately constant upstream of the shock. Then by using an equation of state for an adiabatic flow, and linearizing the steady and inviscid two-dimensional continuity, momentum, and energy equations, we can eliminate (an isotropic) pressure and momentum to find

$$(1 - \bar{W}^2) \frac{\partial \tilde{v}_\xi}{\partial \xi} + \frac{\partial \tilde{v}_\eta}{\partial \eta} = 0. \quad (\text{A1})$$

This equation is identically satisfied if the velocity satisfies the following relations with a defined stream function, ψ ,

$$\begin{aligned} \tilde{v}_\xi &= \frac{\partial \psi}{\partial \eta}, \\ \tilde{v}_\eta &= -(1 - \bar{W}^2) \frac{\partial \psi}{\partial \xi}. \end{aligned} \quad (\text{A2})$$

To find a PDE that describes the evolution of ψ we express the vorticity, defined as $\Omega \equiv \partial \tilde{v}_\eta / \partial \xi - \partial \tilde{v}_\xi / \partial \eta$, in terms of the stream function using Eq. (A2):

$$(1 - \bar{W}^2) \frac{\partial^2 \psi}{\partial \xi^2} + \frac{\partial^2 \psi}{\partial \eta^2} = -\Omega. \quad (\text{A3})$$

The vorticity can then be related to the change in entropy, s , and enthalpy, H , perpendicular to stream lines via Crocco's

theorem [77]:

$$(1 - \bar{W}^2) \frac{\partial^2 \psi}{\partial \xi^2} + \frac{\partial^2 \psi}{\partial \eta^2} = -\Omega = \frac{1}{W} \left(\frac{\partial H}{\partial \eta} - T \frac{\partial s}{\partial \eta} \right). \quad (\text{A4})$$

The sign of the coefficient of $\partial^2 \psi / \partial \xi^2$, and therefore the nature of the PDE, depends on whether the resultant downstream flow is subsonic $\bar{W}_1 < 1$ or supersonic $\bar{W}_1 > 1$. Thus, solutions must be found separately in each case.

Boundary conditions on the velocity components can be found by considering the standard oblique-shock relations. Since the perturbation velocity aligns with the flow, it will perturb the angle of the shock locally by $\sigma(y)$, where y is the direction parallel to the shock front, and x is the direction normal to the shock. This rippling of the shock front will introduce vorticity and thus amplify the initial mode. A linear treatment is consistent provided that the initial vorticity mode is sufficiently weak, such that the amplified, downstream perturbations are still weak relative to the bulk flow.

If the initial vorticity mode is weak, then we assume the upstream temperature to be constant and perturbations to the shock angle to be small. Then by applying the oblique-shock relations to the shock-normal component of the perturbed flow, boundary conditions relating the upstream and downstream velocity perturbations can be found.

Let us define the initial sinusoidal perturbation velocity by

$$\frac{\tilde{v}_{\xi 0}}{W_0} = \epsilon \cos k_0 \eta_0, \quad (\text{A5})$$

where k_0 denotes the wave number of the initial mode, and ϵ the small perturbation amplitude. Then at the shock front, the nulls and peaks of the initial and refracted vorticity modes must match, such that $k_0 \eta_0 = k_1 \eta_1$. Thus, the upstream perturbation velocity can be expressed in terms of downstream quantities separately from the oblique-shock relations.

We assume the initially unknown perturbation to the shock to also be sinusoidal in nature, with yet undetermined amplitude and phase. This can be parameterized by the two unknowns as

$$\sigma = \epsilon (a \cos k_1 \eta_1 + b \sin k_1 \eta_1). \quad (\text{A6})$$

Substituting the sinusoidal vorticity and shock perturbations, Eqs. (A5) and (A6), into the boundary conditions found using the oblique-shock relations, gives the following set of boundary conditions on the velocity perturbations parallel and perpendicular to the mean postshock flow:

$$\begin{aligned} \frac{\tilde{v}_\xi(x=0)}{\epsilon \bar{v}_x} &= \left[\frac{a}{m} \left(1 - 2 \frac{\gamma-1}{\gamma+1} m + m^2 \right) \sin \varphi \left(1 - 2 \frac{\gamma-1}{\gamma+1} m \right) \cos \varphi + \frac{\sin^2 \varphi}{\cos \varphi} \right] \cos \kappa \eta + \left[\frac{b}{m} \left(1 - 2 \frac{\gamma-1}{\gamma+1} m + m^2 \right) \sin \varphi \right] \\ &\times \sin \kappa \eta, \end{aligned} \quad (\text{A7})$$

$$\begin{aligned} \frac{\tilde{v}_\eta(x=0)}{\epsilon \bar{v}_x} &= \left[-\frac{a}{m} \left(1 + \frac{3-\gamma}{\gamma+1} m \right) \frac{\sin^2 \varphi}{\cos \varphi} + a(m-1) \cos \varphi + 2 \left(1 - \frac{\gamma-1}{\gamma+1} m \right) \sin \varphi \right] \cos \kappa \eta \\ &+ \left[-\frac{b}{m} \left(1 + \frac{3-\gamma}{\gamma+1} m \right) \frac{\sin^2 \varphi}{\cos \varphi} + b(m-1) \cos \varphi \right] \sin \kappa \eta, \end{aligned} \quad (\text{A8})$$

where we have dropped subscript $_1$ for denoting downstream quantities, and let $\theta_1 \equiv \varphi$, $k_1 \equiv \kappa$. The unknown constants a and b related to the shock perturbation are to be determined by matching to the stream function solution of Eq. (A4).

To solve Eq. (A4), we first evaluate the inhomogeneous vorticity term on the right hand side. When perturbations are sufficiently weak to justify a linear treatment, the downstream streamlines are approximately straight lines described by $\eta = \text{const}$. Therefore, both the downstream enthalpy H and entropy s are constant along these straight streamlines, retaining their values from the shock front. For weak vorticity perturbations, we may assume the upstream temperature, pressure and density are constant. Therefore, the upstream entropy will also be constant. Oblique shock relations for the change of entropy across the shock [78] and the upstream enthalpy evaluated at the shock can be used to re-express the right-hand side of Eq. (A4) (evaluated at the shock front) as

$$(1 - \bar{W}^2) \frac{\partial^2 \psi}{\partial \xi^2} + \frac{\partial^2 \psi}{\partial \eta^2} = \bar{v}_x m^2 \frac{\cos \varphi}{\cos^2 \theta_0} \frac{\partial}{\partial \eta} \left(\frac{\tilde{v}_{\xi 0}}{W_0} \right) - \bar{v}_x \cos \varphi (m-1)^2 \times \frac{\partial}{\partial \eta} \left(\frac{\tilde{v}_{\xi 0}}{W_0} - \sigma \tan \theta_0 \right). \quad (\text{A9})$$

We then specialize this to our problem by substituting in the sinusoidal perturbations for velocity and to the shock front, Eqs. (A5) and (A6), and using $\tan \varphi = m \tan \theta_0$,

$$(1 - \bar{W}^2) \frac{\partial^2 \psi}{\partial \xi^2} + \frac{\partial^2 \psi}{\partial \eta^2} = \bar{v}_x \epsilon \left(-\kappa \left[\sec \varphi + 2(m-1) \cos \varphi + a \frac{(m-1)^2}{m} \sin \varphi \right] \times \sin \kappa \eta + \kappa b \frac{(m-1)^2}{m} \sin \varphi \cos \kappa \eta \right). \quad (\text{A10})$$

Ribner then finds general solutions of the stream function, ψ , to Eq. (A10) for $\bar{W} \leq 1$ and $\bar{W} \geq 1$, and determines both the arbitrary constants and the two unknowns of the shock perturbation through matching to the boundary conditions Eqs. (A7) and (A8). The perturbation velocity components downstream of the shock can then be evaluated from the stream function using Eq. (A2).

The solutions include velocity perturbations that are aligned with and constant along the downstream resultant flow in the steady frame, and other perturbations that correspond to acoustic or Mach waves. The former are identified as downstream vorticity modes and arise from the particular solutions of Eq. (A10) which correspond to the inhomogeneous vorticity term. Then the velocity perturbations of the downstream vorticity mode can be expressed as the following:

$$\frac{|\tilde{v}^{\text{vorticity}}|}{|\tilde{v}_0|} = S \cos[\kappa_y(y - x \tan \varphi) + \delta_s], \quad (\text{A11})$$

where $\kappa_y = \kappa \cos \varphi = k \cos \theta_0$ and

$$S \equiv \frac{\cos \theta_0}{m} \sqrt{A^2 + B^2}, \quad (\text{A12})$$

$$\delta_s = \arctan \left(\frac{-B}{A} \right). \quad (\text{A13})$$

A and B correspond to terms in the inhomogeneous part of Eq. (A10):

$$(1 - \bar{W}^2) \frac{\partial^2 \psi}{\partial \xi^2} + \frac{\partial^2 \psi}{\partial \eta^2} = -\kappa U \epsilon (A \sin \kappa \eta - B \cos \kappa \eta), \quad (\text{A14})$$

with

$$A \equiv \left[\sec \varphi + 2(m-1) \cos \varphi + a \frac{(m-1)^2}{m} \sin \varphi \right], \quad (\text{A15})$$

$$B \equiv b \frac{(m-1)^2}{m} \sin \varphi. \quad (\text{A16})$$

a and b are the now determined constants describing the perturbation to the shock in Eq. (A6).

For the case where the downstream resultant flow is subsonic, $\bar{W} \leq 1$, Ribner determines these constants to be

$$a = m \frac{CE + DF}{C^2 + D^2}, \quad (\text{A17})$$

$$b = m \frac{CF - DE}{C^2 + D^2}, \quad (\text{A18})$$

where

$$C \equiv \left(\frac{\gamma-1}{\gamma+1} + \frac{3-\gamma}{\gamma+1} m \right) \tan \varphi - \left[(m-1)^2 + \frac{2(m-1)}{\gamma+1} \right] \times \sin \varphi \cos \varphi, \quad (\text{A19})$$

$$D \equiv \frac{\beta_w}{\beta^2} (m-1) [1 + (m-1) \cos^2 \varphi], \quad (\text{A20})$$

$$E \equiv 2 \left(1 - \frac{\gamma-1}{\gamma+1} m \right) + 2(m-1) \frac{\beta_w^2 \cos^2 \varphi}{\beta^2}, \quad (\text{A21})$$

$$F \equiv \frac{\beta_w}{\beta^2} [2(m-1) \sin \varphi \cos \varphi], \quad (\text{A22})$$

$$\beta_w^2 = 1 - \bar{W}^2, \quad (\text{A23})$$

$$\beta^2 = 1 - \bar{v}_x^2. \quad (\text{A24})$$

When $\overline{W} \geq 1$ we find that

$$a = \frac{2m(2\beta_w m + (1 + \gamma + m - \gamma m) \tan \varphi)}{(3m + 1 - \gamma(m - 1)) \tan^2 \varphi + 4\beta_w m \tan \varphi - m(m - 1)(\gamma + 1)}, \quad (\text{A25})$$

$$b = 0. \quad (\text{A26})$$

For our calculation, we acquired the above expression for a , Eq. (A25), from directly matching the $\overline{W} \geq 1$ general solution to the boundary conditions.

-
- [1] A. L. Velikovich, J. G. Wouchuk, C. Huete Ruiz de Lira, N. Metzler, S. Zalesak, and A. J. Schmitt, Shock front distortion and Richtmyer-Meshkov-type growth caused by a small preshock nonuniformity, *Phys. Plasmas* **14**, 072706 (2007).
 - [2] B. A. Hammel, S. W. Haan, D. S. Clark, M. J. Edwards, S. H. Langer, M. M. Marinak, M. V. Patel, J. D. Salmonson, and H. A. Scott, High-mode Rayleigh-Taylor growth in NIF ignition capsules, *High Energy Density Phys.* **6**, 171 (2010).
 - [3] C. R. Weber, D. S. Clark, A. W. Cook, L. E. Busby, and H. F. Robey, Inhibition of turbulence in inertial-confinement-fusion hot spots by viscous dissipation, *Phys. Rev. E* **89**, 053106 (2014).
 - [4] T. Ma, P. K. Patel, N. Izumi, P. T. Springer, M. H. Key, L. J. Atherton, L. R. Benedetti, D. K. Bradley, D. A. Callahan, P. M. Celliers, C. J. Cerjan, D. S. Clark, E. L. Dewald, S. N. Dixit, T. Döppner, D. H. Edgell, R. Epstein, S. Glenn, G. Grim, S. W. Haan *et al.*, Onset of hydrodynamic mix in high-velocity, highly compressed inertial confinement fusion implosions, *Phys. Rev. Lett.* **111**, 085004 (2013).
 - [5] Y. Zhou, J. D. Sadler, and O. A. Hurricane, Instabilities and mixing in inertial confinement fusion, *Annu. Rev. Fluid Mech.* **57**, 197 (2025).
 - [6] Y. Zhou, *Hydrodynamic Instabilities and Turbulence: Rayleigh–Taylor, Richtmyer–Meshkov, and Kelvin–Helmholtz Mixing* (Cambridge University Press, Cambridge, UK, 2024).
 - [7] J. Lindl, Development of the indirect-drive approach to inertial confinement fusion and the target physics basis for ignition and gain, *Phys. Plasmas* **2**, 3933 (1995).
 - [8] W. Hillebrandt and J. C. Niemeyer, Type IA supernova explosion models, *Ann. Rev. Astron. Astro.* **38**, 191 (2000).
 - [9] J. M. Blondin, A. Mezzacappa, and C. DeMarino, Stability of standing accretion shocks, with an eye toward core-collapse supernovae, *Astrophys. J.* **584**, 971 (2003).
 - [10] E. Abdikamalov, A. Zhaksylykov, D. Radice, and S. Berdibek, Shock-turbulence interaction in core-collapse supernovae, *Mon. Not. R. Astron. Soc.* **461**, 3864 (2016).
 - [11] M.-M. Mac Low and R. S. Klessen, Control of star formation by supersonic turbulence, *Rev. Mod. Phys.* **76**, 125 (2004).
 - [12] C. K. W. Tam and H. K. Tanna, Shock associated noise of supersonic jets from convergent-divergent nozzles, *J. Sound Vib.* **81**, 337 (1982).
 - [13] H. Abu-Shawareb, R. Acree, P. Adams, J. Adams, B. Addis, R. Aden, P. Adrian, B. B. Afeyan, M. Aggleton, L. Aghaian, A. Aguirre, D. Aikens, J. Akre, F. Albert, M. Albrecht, B. J. Albright, J. Albritton, J. Alcalá, C. Alday, D. A. Alessi *et al.*, Lawson criterion for ignition exceeded in an inertial fusion experiment, *Phys. Rev. Lett.* **129**, 075001 (2022).
 - [14] S. W. Haan, J. D. Lindl, D. A. Callahan, D. S. Clark, J. D. Salmonson, B. A. Hammel, L. J. Atherton, R. C. Cook, M. J. Edwards, S. Glenzer, A. V. Hamza, S. P. Hatchett, M. C. Herrmann, D. E. Hinkel, D. D. Ho, H. Huang, O. S. Jones, J. Kline, G. Kyrala, O. L. Landen *et al.*, Point design targets, specifications, and requirements for the 2010 ignition campaign on the national ignition facility, *Phys. Plasmas* **18**, 051001 (2011).
 - [15] H. F. Robey, T. R. Boehly, P. M. Celliers, J. H. Eggert, D. Hicks, R. F. Smith, R. Collins, M. W. Bowers, K. G. Krauter, P. S. Datte, D. H. Munro, J. L. Milovich, O. S. Jones, P. A. Michel, C. A. Thomas, R. E. Olson, S. Pollaine, R. P. J. Town, S. Haan, D. Callahan *et al.*, Shock timing experiments on the National Ignition Facility: Initial results and comparison with simulation, *Phys. Plasmas* **19**, 042706 (2012).
 - [16] S. Davidovits, C. Federrath, R. Teyssier, K. S. Raman, D. C. Collins, and S. R. Nagel, Turbulence generation by shock interaction with a highly nonuniform medium, *Phys. Rev. E* **105**, 065206 (2022).
 - [17] S. Davidovits, C. R. Weber, and D. S. Clark, Modeling ablator grain structure impacts in ICF implosions, *Phys. Plasmas* **29**, 112708 (2022).
 - [18] G. J. Li and S. Davidovits, Microphysics of shock-grain interaction for inertial confinement fusion ablaters in a fluid approach, *Phys. Rev. E* **110**, 035206 (2024).
 - [19] R. Sacks and D. Darling, Direct drive cryogenic ICF capsules employing D-T wetted foam, *Nucl. Fusion* **27**, 447 (1987).
 - [20] J. D. Moody, B. J. MacGowan, S. H. Glenzer, R. K. Kirkwood, W. L. Kruer, D. S. Montgomery, A. J. Schmitt, E. A. Williams, and G. F. Stone, Experimental investigation of short scalelength density fluctuations in laser-produced plasmas, *Phys. Plasmas* **7**, 2114 (2000).
 - [21] S. Root, T. A. Haill, J. M. D. Lane, A. P. Thompson, G. S. Grest, D. G. Schroen, and T. R. Mattsson, Shock compression of hydrocarbon foam to 200 GPa: Experiments, atomistic simulations, and mesoscale hydrodynamic modeling, *J. Appl. Phys.* **114**, 103502 (2013).
 - [22] A. D. Kotelnikov and D. C. Montgomery, Shock induced turbulence in composite materials at moderate Reynolds numbers, *Phys. Fluids* **10**, 2037 (1998).
 - [23] C. Huete, J. G. Wouchuk, B. Canaud, and A. L. Velikovich, Analytical linear theory for the shock and re-shock of isotropic density inhomogeneities, *J. Fluid Mech.* **700**, 214 (2012).
 - [24] S. R. Nagel, K. S. Raman, C. M. Huntington, S. A. MacLaren, P. Wang, M. A. Barrios, T. Baumann, J. D. Bender, L. R. Benedetti, D. M. Doane, S. Felker, P. Fitzsimmons, K. A. Flippo, J. P. Holder, D. N. Kaczala, T. S. Perry, R. M. Seugling, L. Savage, and Y. Zhou, A platform for studying

- the Rayleigh-Taylor and Richtmyer-Meshkov instabilities in a planar geometry at high energy density at the National Ignition Facility, *Phys. Plasmas* **24**, 072704 (2017).
- [25] S. R. Nagel, K. S. Raman, C. M. Huntington, S. A. MacLaren, P. Wang, J. D. Bender, S. T. Prisbrey, and Y. Zhou, Experiments on the single-mode Richtmyer-Meshkov instability with Reshock at high energy densities, *Phys. Plasmas* **29**, 032308 (2022).
- [26] J. D. Bender, O. Schilling, K. S. Raman, R. A. Managan, B. J. Olson, S. R. Copeland, C. L. Ellison, D. J. Erskine, C. M. Huntington, B. E. Morgan, S. R. Nagel, S. T. Prisbrey, B. S. Pudliner, P. A. Sterne, C. E. Wehrenberg, and Y. Zhou, Simulation and flow physics of a shocked and Reshocked high-energy-density mixing layer, *J. Fluid Mech.* **915**, A84 (2021).
- [27] E. Leinov, G. Malamud, Y. Elbaz, L. A. Levin, G. Ben-Dor, D. Shvarts, and O. Sadot, Experimental and numerical investigation of the Richtmyer-Meshkov instability under re-shock conditions, *J. Fluid Mech.* **626**, 449 (2009).
- [28] R. E. Pudritz and N. K. R. Kevlahan, Shock interactions, turbulence and the origin of the stellar mass spectrum, *Phil. Trans. R. Soc. A* **371**, 20120248 (2013).
- [29] M. M. Kupilas, C. J. Wareing, J. M. Pittard, and S. A. E. G. Falle, Interactions of a shock with a molecular cloud at various stages of its evolution due to thermal instability and gravity, *Mon. Not. Roy. Astron. Soc.* **501**, 3137 (2021).
- [30] A. Grzona and H. Olivier, Shock train generated turbulence inside a nozzle with a small opening angle, *Exp. Fluids* **51**, 621 (2011).
- [31] H. S. Ribner, Acoustic energy flux from shock-turbulence interaction., *J. Fluid Mech.* **35**, 299 (1969).
- [32] H. S. Ribner, Spectra of noise and amplified turbulence emanating from shock-turbulence interaction, *AIAA J.* **25**, 436 (1987).
- [33] H. S. Ribner, Comment on “Experimental study of a normal shock/homogeneous turbulence interaction,” *AIAA J.* **36**, 494 (1998).
- [34] H. S. Ribner, Convection of a pattern of vorticity through a shock wave, Tech. Rep. 1164 (National Advisory Committee for Aeronautics, Washington, D.C., 1953).
- [35] H. S. Ribner, Shock-turbulence interaction and the generation of noise, Tech. Rep. 1233 (National Advisory Committee for Aeronautics, Washington, D.C., 1954).
- [36] L. S. G. Kovasnay, Turbulence in supersonic flow, *J. Aeronaut. Sci.* **20**, 657 (1953).
- [37] J. G. Wouchuk, C. Huete Ruiz de Lira, and A. L. Velikovich, Analytical linear theory for the interaction of a planar shock wave with an isotropic turbulent vorticity field, *Phys. Rev. E* **79**, 066315 (2009).
- [38] F. K. Moore, Unsteady oblique interaction of a shock wave with a plane disturbance, Tech. Rep. 1165 (National Advisory Committee for Aeronautics, Washington, D.C., 1953).
- [39] K. Mahesh, S. Lee, S. K. Lele, and P. Moin, The interaction of an isotropic field of acoustic waves with a shock wave, *J. Fluid Mech.* **300**, 383 (1995).
- [40] K. Mahesh, S. K. Lele, and P. Moin, The influence of entropy fluctuations on the interaction of turbulence with a shock wave, *J. Fluid Mech.* **334**, 353 (1997).
- [41] S. Jamme, J. B. Cazalbou, F. Torres, and P. Chassaing, Direct numerical simulation of the interaction between a shock wave and various types of isotropic turbulence, *Flow, Turbul. Combust.* **68**, 227 (2002).
- [42] J. Ryu and D. Livescu, Turbulence structure behind the shock in canonical shock-vortical turbulence interaction, *J. Fluid Mech.* **756**, R1 (2014).
- [43] C. H. Chen and D. A. Donzis, Shock-turbulence interactions at high turbulence intensities, *J. Fluid Mech.* **870**, 813 (2019).
- [44] S. Barre, D. Alem, and J. P. Bonnet, Experimental study of a normal shock/homogeneous turbulence interaction, *AIAA J.* **34**, 968 (1996).
- [45] J. Larsson and S. K. Lele, Direct numerical simulation of canonical shock/turbulence interaction, *Phys. Fluids* **21**, 126101 (2009).
- [46] S. Lee, S. K. Lele, and P. Moin, Direct numerical simulation of isotropic turbulence interacting with a weak shock wave, *J. Fluid Mech.* **251**, 533 (1993).
- [47] S. Lee, S. K. Lele, and P. Moin, Interaction of isotropic turbulence with shock waves: Effect of shock strength, *J. Fluid Mech.* **340**, 225 (1997).
- [48] J. Larsson, I. Bermejo-Moreno, and S. K. Lele, Reynolds- and Mach-number effects in canonical shock-turbulence interaction, *J. Fluid Mech.* **717**, 293 (2013).
- [49] K. Mahesh, S. K. Lele, and P. Moin, The response of anisotropic turbulence to rapid homogeneous one-dimensional compression, *Phys. Fluids* **6**, 1052 (1994).
- [50] R. Hannappel and R. Friedrich, DNS of a $M = 2$ shock interacting with isotropic turbulence, in *Direct and Large-Eddy Simulation I: Selected Papers from the First ERCOFTAC Workshop on Direct and Large-Eddy Simulation*, edited by P. R. Voke, L. Kleiser, and J.-P. Chollet (Springer Netherlands, Dordrecht, 1994), pp. 359–373.
- [51] S. Davidovits and N. J. Fisch, Preferential turbulence enhancement in two-dimensional compressions, *Phys. Rev. E* **102**, 053213 (2020).
- [52] P. Sagaut and C. Cambon, *Homogeneous Turbulence Dynamics* (Springer, Cham, 2018).
- [53] K.-S. Choi and J. L. Lumley, The return to isotropy of homogeneous turbulence, *J. Fluid Mech.* **436**, 59 (2001).
- [54] S. Davidovits and N. J. Fisch, Understanding turbulence in compressing plasma as a quasi-EOS, *Phys. Plasmas* **26**, 062709 (2019).
- [55] S. Davidovits and N. J. Fisch, Sudden viscous dissipation of compressing turbulence, *Phys. Rev. Lett.* **116**, 105004 (2016).
- [56] H. Fetsch and N. J. Fisch, Enhancement to fusion reactivity in sheared flows, [arXiv:2410.03590](https://arxiv.org/abs/2410.03590).
- [57] B. M. Haines, R. C. Shah, J. M. Smidt, B. J. Albright, T. Cardenas, M. R. Douglas, C. Forrest, V. Y. Glebov, M. A. Gunderson, C. E. Hamilton, K. C. Henderson, Y. Kim, M. N. Lee, T. J. Murphy, J. A. Oertel, R. E. Olson, B. M. Patterson, R. B. Randolph, and D. W. Schmidt, Observation of persistent species temperature separation in inertial confinement fusion mixtures, *Nat. Commun.* **11**, 544 (2020).
- [58] B. Bachmann, S. A. MacLaren, S. Bhandarkar, T. Briggs, D. Casey, L. Divol, T. Döppner, D. Fittinghoff, M. Freeman, S. Haan, G. N. Hall, B. Hammel, E. Hartouni, N. Izumi, V. Geppert-Kleinrath, S. Khan, B. Kozioziemski, C. Krauland, O. Landen, D. Mariscal *et al.*, Measurement of dark ice-ablator mix in inertial confinement fusion, *Phys. Rev. Lett.* **129**, 275001 (2022).

- [59] G. N. Hall, C. R. Weber, V. A. Smalyuk, O. L. Landen, C. Troselle, A. Pak, E. Hartouni, E. Marley, T. Ebert, D. K. Bradley, W. Hsing, R. Tommasini, N. Izumi, S. L. Pape, L. Divol, C. M. Krauland, N. Thompson, E. R. Casco, M. J. Ayers, S. R. Nagel *et al.*, Measurement of mix at the fuel-ablator interface in indirectly driven capsule implosions on the National Ignition Facility, *Phys. Plasmas* **31**, 022702 (2024).
- [60] S. J. Ali, P. M. Celliers, S. Haan, T. R. Boehly, N. Whiting, S. H. Baxamusa, H. Reynolds, M. A. Johnson, J. D. Hughes, B. Watson, H. Huang, J. Biener, K. Engelhorn, V. A. Smalyuk, and O. L. Landen, Probing the seeding of hydrodynamic instabilities from nonuniformities in ablator materials using 2D velocimetry, *Phys. Plasmas* **25**, 092708 (2018).
- [61] A. B. Zylstra, A. L. Kritcher, O. A. Hurricane, D. A. Callahan, J. E. Ralph, D. T. Casey, A. Pak, O. L. Landen, B. Bachmann, K. L. Baker, L. Berzak Hopkins, S. D. Bhandarkar, J. Biener, R. M. Bionta, N. W. Birge, T. Braun, T. M. Briggs, P. M. Celliers, H. Chen, C. Choate *et al.*, Experimental achievement and signatures of ignition at the National Ignition Facility, *Phys. Rev. E* **106**, 025202 (2022).
- [62] A. L. Kritcher, A. B. Zylstra, D. A. Callahan, O. A. Hurricane, C. R. Weber, D. S. Clark, C. V. Young, J. E. Ralph, D. T. Casey, A. Pak, O. L. Landen, B. Bachmann, K. L. Baker, L. Berzak Hopkins, S. D. Bhandarkar, J. Biener, R. M. Bionta, N. W. Birge, T. Braun, T. M. Briggs *et al.*, Design of an inertial fusion experiment exceeding the Lawson criterion for ignition, *Phys. Rev. E* **106**, 025201 (2022).
- [63] D. S. Clark, A. Allen, S. H. Baxamusa, J. Biener, M. M. Biener, T. Braun, S. Davidovits, L. Divol, W. A. Farmer, T. Fehrenbach, C. Kong, M. Millot, J. Milovich, A. Nikroo, R. C. Nora, A. E. Pak, M. S. Rubery, M. Stadermann, P. Sterne, C. R. Weber *et al.*, Modeling ablator defects as a source of mix in high-performance implosions at the National Ignition Facility, *Phys. Plasmas* **31**, 062706 (2024).
- [64] S. Davidovits and N. J. Fisch, Bulk hydrodynamic stability and turbulent saturation in compressing hot spots, *Phys. Plasmas* **25**, 042703 (2018).
- [65] C. R. Weber, D. S. Clark, A. W. Cook, D. C. Eder, S. W. Haan, B. A. Hammel, D. E. Hinkel, O. S. Jones, M. M. Marinak, J. L. Milovich, P. K. Patel, H. F. Robey, J. D. Salmonson, S. M. Sepke, and C. A. Thomas, Three-dimensional hydrodynamics of the deceleration stage in inertial confinement fusion, *Phys. Plasmas* **22**, 032702 (2015).
- [66] L. D. Landau and E. M. Lifshitz, *Fluid Mechanics* (Elsevier, Amsterdam, 2008).
- [67] S. P. D'Iakov, The interaction of shock waves with small perturbations. I, *Sov. J. Exper. Theor. Phys.* **6**, 729 (1958).
- [68] V. M. Kontorovich, Concerning the stability of shock waves, *Sov. J. Exper. Theor. Phys.* **6**, 1179 (1958).
- [69] J. F. McKenzie and K. O. Westphal, Interaction of linear waves with oblique shock waves, *Phys. Fluids* **11**, 2350 (1968).
- [70] L. J. Perkins, D. D. M. Ho, B. G. Logan, G. B. Zimmerman, M. A. Rhodes, D. J. Strozzi, D. T. Blackfield, and S. A. Hawkins, The potential of imposed magnetic fields for enhancing ignition probability and fusion energy yield in indirect-drive inertial confinement fusion, *Phys. Plasmas* **24**, 062708 (2017).
- [71] C. A. Walsh, K. McGlinchey, J. K. Tong, B. D. Appelbe, A. Crilly, M. F. Zhang, and J. P. Chittenden, Perturbation modifications by pre-magnetisation of inertial confinement fusion implosions, *Phys. Plasmas* **26**, 022701 (2019).
- [72] M. F. Zhang, M. W. Kunz, J. Squire, and K. G. Klein, Extreme heating of minor ions in imbalanced solar-wind turbulence, *Astrophys. J.* **979**, 121 (2025).
- [73] J. T. Coburn, C. H. K. Chen, and J. Squire, A measurement of the effective mean free path of solar wind protons, *J. Plasma Phys.* **88**, 175880502 (2022).
- [74] C. H. K. Chen, S. D. Bale, J. W. Bonnell, D. Borovikov, T. A. Bowen, D. Burgess, A. W. Case, B. D. G. Chandran, T. D. de Wit, K. Goetz, P. R. Harvey, J. C. Kasper, K. G. Klein, K. E. Korreck, D. Larson, R. Livi, R. J. MacDowall, D. M. Malaspina, A. Mallet, M. D. McManus *et al.*, The evolution and role of solar wind turbulence in the inner heliosphere, *Astrophys. J. Supp.* **246**, 53 (2020).
- [75] H. C. Zhuang and C. T. Russell, Interaction of small-amplitude fluctuations with a strong magnetohydrodynamic shock, *Phys. Fluids* **25**, 748 (1982).
- [76] L. Zhao, X. Zhu, A. Silwal, G. P. Zank, and A. Pitña, Theory and observations of the interaction between magnetohydrodynamic waves and shocks, *Proc. Natl. Acad. Sci. USA* **122**, e2425668122 (2025).
- [77] H. Liepmann and A. Roshko, *Elements of Gasdynamics*, Dover Books on Aeronautical Engineering Series (Dover Publications, Oxford, UK, 2001).
- [78] The staff of the Ames 1-by 3-foot supersonic wind-tunnel section, Notes and Tables for use in the analysis of supersonic flow, Tech. Rep. 1428 (National Advisory Committee for Aeronautics, Washington, D.C., 1947).